Energy growth in Hagen-Poiseuille flow of Herschel-Bulkley fluid

Hocine Bentrad, Ahmed Esmael, Chérif Nouar, Alain Lefevre, Noureddine Ait-Messaoudene

Energy growth in Hagen-Poiseuille flow of Herschel-Bulkley fluid

Hocine Bentrad, [a] Ahmed Esmael, [b] Chérif Nouar[1] [c]
Alain Lefevre [c] and Noureddine Ait-Messaoudene [a c]

[a] *LApEH, Université Saad Dahleb, Blida, Algeria*

[b] *Mechanical Engineering Department, El-Mergib University, Libya*

[c] *LEMTA, UMR* 7563 *(CNRS),* 2*, avenue de la forêt de Haye, BP* 160*,* 54504 *Vandoeuvre Cedex, France*

[d] *Department of Mechanical Engineering, Faculty of Engineering, University of Hail, PO Box 2440 Hail, Saudi Arabia*

1

Abstract

Linear stability of Poiseuille flow of Herschel-Bulkley fluid in a cylindrical pipe is studied using modal and non-modal approaches. The first part of the present study thus deals with the classical normal mode approach in which the resulting eigenvalue problem is solved using a Chebyshev collocation method. Within the considered range of parameters, the modal-linear theory predicts that perturbations are dumped exponentially. In the second part, the effect of the rheological behaviour of the fluid on the pseudospectra and the most amplified perturbations is investigated. At very low Herschel-Bulkley number ($Hb << 1$), the optimal perturbation consists of almost streamwise vortices, and the amplification of the kinetic energy is provided by the lift-up mechanism. In contrast, for sufficiently large values of Hb, the optimal perturbation is axisymmetric and the growth of the kinetic energy is provided by the Orr-mechanism. For intermediate values of Hb, the optimal perturbation is oblique. The amplification of such perturbation is due to a synergy between Orr and lift-up mechanisms. In the last part of the study, the maximal value of the Reynolds number, Re_{cE}, below which the perturbation energy decreases monotonically with time is computed for a large range of Hb. Asymptotic behaviors of Re_{cE} for $Hb << 1$ and $Hb >> 1$ are established. The influence of the terms arising from the viscosity perturbation is highlighted throughout this study.

Key words: Herschel-Bulkley fluid, cylindrical pipe, transient-growth, energy method

[1] Corresponding author: Tel: 00 33 3 83 59 55 95; Fax: 00 33 3 83 59 56 16; E-mail address: cherif.nouar@univ-lorraine.fr

1 Introduction

The first step in the study of the transition to turbulence consists in considering the linearized equations and the starting point is the standard normal mode approach. Existence of unstable modes means that there is an exponential growth of infinitesimal perturbation and the eigenfunction represents the pattern that appear in early stage of transition. The predictions of the normal mode analysis match the laboratory experiments for some flows, notably Taylor Couette flow and Rayleigh-Bénard convection. For other flows, such as, open parallel shear flows, the normal mode approach fails to match the experiments. The failure of the normal mode linear stability analysis to describe the early stage of transition is attributed in part to the non-normal nature of the linearized equations, i.e. their eigenfunctions are not orthogonal. The non-normal nature manifests itself by a transient growth of perturbations and a large receptivity to ambient disturbances. The amplification of the kinetic energy of the perturbation may reach a significant amplitude that can trigger nonlinear mechanisms before its long time decay due to viscous effects [1]. The physical mechanism behind the transient growth is related to the inviscid vortex tilting mechanism in the presence of base flow shear.
The Orr-mechanism [2] and the lift-up mechanism [3], [4], [5] are two such commonly identified disturbance growth phenomena in a shear flow. The Orr-mechanism involves disturbance field that consists of spanwise-uniform vortices initially tilted against the direction of the base flow. The disturbance is then sheared and tilted. Its kinetic energy is amplified by the base shear via the working of the Reynolds stress. In the lift-up mechanism, streamwise uniform vortices superimposed on a parallel shear flow lift up fluid at low velocity from the wall and push down towards the wall fluid with high velocity. Hence, elongated streaks with high and low velocity are generated.
For arbitrary 3D perturbations, both Orr and lift-up mechanisms are operating, but in a hierarchical manner. The Orr mechanism generates a transient normal-wall velocity, which in turn creates by the lift-up mechanism streamwise streaks that decay slowly by viscosity [6].
The optimal perturbation, i.e. the initial perturbation that undergoes the largest amplification of the kinetic energy, is a fundamental concept of the linear stability theory [7]. In simple shear flows, such as Couette, Poiseuille or Hagen-Poiseuille flows, the optimal perturbation takes the form of streamwise or quasi streamwise vortices which evolve, via lift-up effect, into spanwise-periodic streaks (regions of positive and negative streamwise velocity) elongated along the main flow direction. A review on the lift-up process in shear flows can be found in [8]

Comparatively to the Newtonian case, very few studies have been devoted to the transient growth in non-Newtonian fluid flows. This is perhaps not sur-

prising, given the inherent complexities involved. Non-Newtonian fluids can be divided in three broad groups: (i) time-independent fluids, for which the viscosity is solely dependent on the instantaneous second invariant of the strain-rate tensor; (ii) viscoelastic fluids, for which stresses depend on the flow history and (iii) time-dependent fluids, for which the strain-rate is a function of both the magnitude and the duration of the applied stress.

Transient growth analysis of inertialess Couette and Poiseuille flows of Oldroyd-B models was studied by Jovanovic and Kumar [9], [10]. It is shown that the presence of elasticity can produce significant energy amplification. The most amplified disturbances tend to be elongated in the streamwise direction. The mechanism responsible for the energy amplification is related to the stretching of the polymer molecules by the background shear which results in a lift-up of the disturbances. In the case of inertia dominated channel flow of viscoelastic fluids modeled by Oldroyd-B and FENE-P closures, Zhang et al. [11] showed that the ratio between the polymer relaxation time and the characteristic time of instability plays a key role on the energy amplification.

Studies on non-modal transient growth in viscosity-stratified fluid flows were recently reviewed by Govindarajan and Sahu [12]. In the present study, we focus on purely viscous (inelastic) shear-thinning fluid flows. The mean features of such fluid flows are: (i) an increase of the wall shear-rate with increasing shear-thinning effects, (ii) a viscosity stratification and (iii) an anisotropy of the shear-stress tensor perturbation which arises from the viscosity perturbation. Chikkadi *et al.* [13] considered the case of plane Poiseuille flow of a Carreau fluid, without taking into account for the anisotropic nature of the shear-stress disturbance tensor. Rather, unexpectedly, the authors found that the transient growth is relatively unaffected by the viscosity gradient. This problem has been revisited by Nouar et al. [14] , and obtained a substantial increase of the transient growth when the viscosity perturbation is taken into account. The optimal perturbation is analogous to that of Newtonian fluids, i.e. longitudinal streamwise vortices which transform into streaks by the lift-up mechanism. Similar results are also obtained in the case of pipe flow of shear-thinning fluids [15]. In the case of the plane Couette flow, the shear-thinning effects reduce only to the anisotropy of the shear-stress tensor perturbation. A significant increase of the transient growth is observed [16]. However, the optimal perturbation remains similar to that for a Newtonian fluid.

Studies dealing with the transient growth in yield stress shear-thinning fluids are very limited. Non-modal stability in plane Poiseuille flow of a yield stress fluid was studied by Nouar et al. [17]. The rheological behavior of the fluid is described by the Bingham model. Comparatively to pure shear-thinning fluids

a fundamental additional parameter intervenes in the problem: the Bingham or the generalized Bingham number, B, which is the ratio of the yield to viscous stresses. This additional parameter will modify the viscosity stratification, the wall shear rate, the anisotropy of the perturbation stress tensor and the geometry of the yielded zone, where the exchange between the base flow and the perturbation occurs. Nouar et al. [17] found that a large amplification of the kinetic energy of the perturbation can be obtained for such fluid flows. At small B, the optimal perturbation is in the form of streamwise uniform vortices, whereas for large B, the optimal transient growth occurs for an oblique wave. Similar results were also obtained by Liu & Liu [18] in the case of Hagen-Poiseuille flow of a Bingham fluid. However, in these studies the physical mechanisms associated with the obliquity of the optimal perturbation are not provided. The influence of the viscosity stratification and that of the anisotropy of the perturbation shear-stress tensor is not clarified.

The objective of the present work is to provide a comprehensive description of the temporal linear stability analysis of Hagen-Poiseuille flow of a shear-thinning yield stress fluid. The rheological behavior of the fluid is described by the Herschel-Bulkley which is used generally in the rheological analysis of yield stress fluids. The goal is to clarify the influence of the viscosity stratification and that of the anisotropy of the stress-tensor perturbation. The structure of the paper is as follows. The governing equations and the base flows details are presented in Sec. 2 and 3 respectively. The linear stability problem is formulated in Sec. 4. The concept of tangent viscosity is introduced. The results of the modal approach and the behavior of the least stable mode are discussed in Sec. 5. The eigenvalue spectra are quite similar to those obtained in Newtonian fluids. Nevertheless, we show that for axisymmetric disturbances, the influence of the yield stress on eigenvalue spectra is very weak. An interpretation based on the tangent viscosity is given. The nonnormality of the linear operators is characterized by the ϵ-pseudospectra and the numerical range in Sec. 6. The results of the energy growth, the optimal perturbations structures and the energy growth scaling are also provided in Sec. 6. The influence of tangent viscosity on the transient growth mechanism is highlighted. The energy stability analysis is presented in Sec. 7. Finally, the summary and conclusions are provided in Sec. 8.

2 Governing equations

The flow of an incompressible shear-thinning fluid with a yield stress $\hat{\tau}_0$ in a circular duct of radius $\hat{R}$ is considered. A constant pressure-gradient $\dfrac{\partial \hat{P}}{\partial \hat{z}}$ is imposed in the axial direction $\boldsymbol{e}_z$. The governing equations in dimensionless

form are:

$$\boldsymbol{\nabla} \cdot \boldsymbol{U} = 0, \tag{1}$$

$$\frac{\partial \boldsymbol{U}}{\partial t} + \boldsymbol{U} \cdot \boldsymbol{\nabla} \boldsymbol{U} = -\boldsymbol{\nabla} P + \boldsymbol{\nabla} \cdot \boldsymbol{\tau} \ , \tag{2}$$

where $\boldsymbol{U}$ is the velocity, P the pressure and $\boldsymbol{\tau}$ the deviatoric of the extra stress tensor. The velocity vector $\boldsymbol{U}$ is of the form $\boldsymbol{U} = U\boldsymbol{e}_r + V\boldsymbol{e}_\theta + W\boldsymbol{e}_z$, where U, V, W are the velocity components and $\boldsymbol{e}_r$, $\boldsymbol{e}_\theta$, $\boldsymbol{e}_z$ are unit vectors in the radial r, circumferential θ and axial z directions respectively. The above equations are non-dimensionalized using the radius of the pipe $\hat{R}$ as the length scale, maximum velocity $\hat{W}_0$ of the basic flow as velocity scale and $\hat{\rho}\hat{W}_0^2$ as stress and pressure scale. The dimensional quantities are denoted with a hat symbol.
The rheological behavior of the fluid is assumed to be described by the Herschel-Bulkley model, which is more realistic than Bingham law. According to [19], the material structure that resists deformation and leads to the yield stress is typically not completely destroyed at $\hat{\tau} = \hat{\tau}_0$. The structure persists post-yield and renders the viscosity shear-rate dependent. For several viscoplastic fluids, the corresponding flow curve is well fitted by the Herschel-Bulkley model. Using the Von-Mises criterion, the scaled constitutive equations are

$$\boldsymbol{\tau} = \frac{1}{Re}\mu\dot{\boldsymbol{\gamma}} \quad \Longleftrightarrow \quad \tau_{_{II}} > \frac{Hb}{Re}, \tag{3}$$

$$\dot{\gamma}_{_{II}} = 0 \quad \Longleftrightarrow \quad \tau_{_{II}} \leq \frac{Hb}{Re}, \tag{4}$$

where $\dot{\gamma}_{_{II}}$ and $\tau_{_{II}}$ are the second invariant of the strain rate tensor $\dot{\boldsymbol{\gamma}}$ and of the deviatoric of the extras stress tensor $\boldsymbol{\tau}$ respectively, given by

$$\dot{\gamma}_{_{II}} = \left[\frac{1}{2}\dot{\gamma}_{ij}\dot{\gamma}_{ij}\right]^{1/2} \quad , \quad \tau_{II} = \left[\frac{1}{2}\dot{\tau}_{ij}\tau_{ij}\right]^{1/2} \tag{5}$$

and $\dot{\gamma}_{ij} = U_{i,j} + U_{j,i}$. The dimensionless effective viscosity μ is defined by

$$\mu = \left[\frac{Hb}{\dot{\gamma}_{_{II}}} + \left(\dot{\gamma}_{_{II}}\right)^{n-1}\right]. \tag{6}$$

The Herschel-Bulkley Hb and the Reynolds Re numbers derived from the non-dimensional governing equations, are defined using a generalized viscosity $\hat{\mu}_{gen} = \hat{K}\left(\hat{W}_0/\hat{R}\right)^{n-1}$. They are given by

$$Hb = \frac{\hat{\tau}_0}{\hat{K}[\hat{W}_0/\hat{R}]^n} \quad , \quad Re = \frac{\hat{\rho}\ \hat{R}^n\ \hat{W}_0^{2-n}}{\hat{K}}, \tag{7}$$

where $\hat{\tau}_0$ is the yield stress, $\hat{K}$ the consistency and n the flow behavior index.

3 Base flow

The base flow is a one directional shear flow, $\boldsymbol{U} = \boldsymbol{U}_b = W_b(r)\boldsymbol{e}_z$ driven by a constant pressure gradient. The subscript b means base flow. The only non zero elements of the strain rate tensor are off-diagonal $\dot{\gamma}_{rz,b} = \dot{\gamma}_{zr,b}$, so that the deviatoric stress tensor elements are all zero except for $\tau_{rz,b} = \tau_{zr,b}$. The momentum equations reduce to:

$$0 = -\frac{dP}{dz} + \frac{1}{r}\frac{d}{dr}\left(r\tau_{rz}\right), \tag{8}$$

where $\tau_{rz,b}$ is given by:

$$\tau_{rz,b} = \frac{1}{Re}\left[sgn\left(\frac{dW_b}{dr}\right)Hb + \left|\frac{dW_b}{dr}\right|^{n-1}\frac{dW_b}{dr}\right] \quad \Leftrightarrow \quad \tau_{rz,b} > \frac{Hb}{Re}, \tag{9}$$

$$\frac{dW_b}{dr} = 0 \quad \Leftrightarrow \quad \tau_{rz,b} \leq \frac{Hb}{Re}. \tag{10}$$

Here, *sgn* mean sign of the argument. Integration of (8) combined with (9, 10) and the non-slip boundary condition at the wall gives:

$$P_b(z) = \frac{-2\,Hb}{Re\,r_0}z + const, \tag{11}$$

$$W_b = \begin{cases} 1 & ; \quad 0 \leq r \leq r_0 \\ 1 - \left(\frac{r-r_0}{1-r_0}\right)^{\frac{n+1}{n}} & ; \quad r_0 \leq r \leq 1, \end{cases} \tag{12}$$

where r_0 is the dimensionless radius of the plug zone. The basic flow (Fig. 1) is characterized by a central region of radius r_0 moving as a rigid solid, i.e. a plug zone which is surrounded by a yielded region where the viscosity μ_b varies nonlinearly with the shear rate:

$$\mu_b = \frac{Hb}{|dW_b/dr|} + |dW_b/dr|^{n-1}. \tag{13}$$

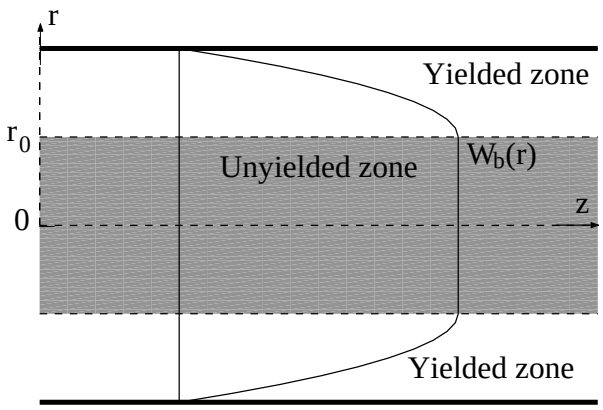

Fig. 1. shematic representation of the base flow.

The viscosity stratification is more pronounced as r_0 is higher or n is lower, as it is shown in Fig. 2. The wall shear-rate, dW_b/dr at $r = 1$, increases as the width of the yielded zone is reduced or as the shear-thinning index decreases.

It is worthy to note that the yield surface $r = r_0$ is not a material surface. The variation of r_0 as function of Hb and n is determined on one hand from the integration of (8) and on the other hand from the constitutive equation:

$$|\tau_w| = \frac{Hb}{r_0\, Re} \quad \text{and} \quad |\tau_w| = \frac{1}{Re}\left[Hb + \left(\frac{n+1}{n}\right)^n \frac{1}{(1-r_0)^{1+n}}\right] \tag{14}$$

From (14) it can be shown that the radius of the yield surface is solution of the following equation

$$Hb\,(1-r_0)^{n+1} - \left(\frac{n+1}{n}\right)^n r_0 = 0\,, \tag{15}$$

For low and large Hb, the following asymptotic behaviors are derived:

$$r_0 \approx \left(\frac{n}{n+1}\right)^n Hb - (n+1)\left(\frac{n}{n+1}\right)^{2n} Hb^2 \quad \text{as} \quad Hb \to 0, \tag{16}$$

$$r_0 \approx 1 - \left(\frac{n+1}{n}\right)^{\frac{n}{n+1}} \left(\frac{1}{Hb}\right)^{\frac{1}{n+1}} \quad \text{as} \quad Hb \to \infty \tag{17}$$

Finally, the base flow depends on two dimensionless parameters, n and Hb or n and r_0. The objective of the present work is to examine the influence of n and Hb on the stability of the Hagen-Poiseuille flow of a Herschel-Bulkley

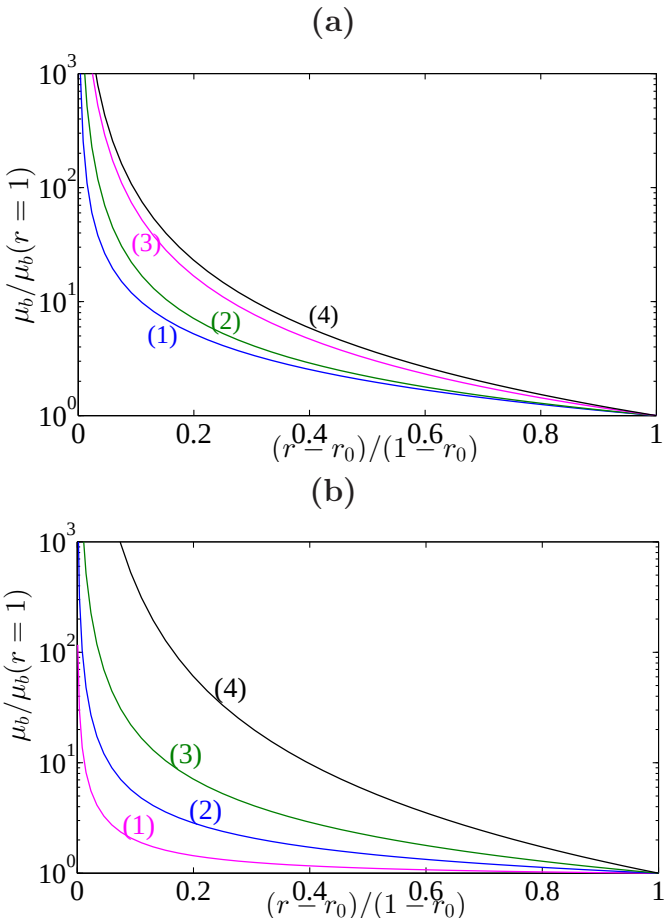

Fig. 2. Viscosity profiles between the yield surface and the wall. **(a)** Influence of the radius of the plug zone on the viscosity stratification for $n = 0.5$: (1) $r_0 = 0.01$, $Hb = 0.0176$; (2) $r_0 = 0.1$, $Hb = 0.203$; (3) $r_0 = 0.5$, $Hb = 2.45$; (4) $r_0 = 0.8$, $Hb = 15.49$. **(b)** Influence of the shear-thinning index with $r_0 = 0.1$: (1) $n = 1$; (2) $n = 0.7$; (3) $n = 0.5$; (4) $n = 0.3$.

fluid with respect to infinitesimal perturbations. This influence arises from four different effects: (i) variation of the yielded zone, where the exchange of energy between the perturbation and the base flow occurs; (ii) variation of the axial velocity gradient dW_b/dr; (iii) viscosity stratification and (iv) nonlinear variation of the viscosity with the shear rate. The contribution of each of these effects on the flow stability will be highlighted whenever possible.

4 Linear stability analysis

An infinitesimal perturbation $(\epsilon \mathbf{u}', \epsilon p')$, with $\epsilon \ll 1$, is imposed on the base flow $(\boldsymbol{U}_b, P_b)$. The perturbed flow is given by:

$$(\boldsymbol{U}_b + \epsilon \boldsymbol{u}', P_b + \epsilon\, p') = (\epsilon\, u', \epsilon\, v', W_b + \epsilon\, w', P_b + \epsilon p')\,. \tag{18}$$

Wherever the yield stress is exceeded, i.e. $\tau > Hb/Re$, the effective viscosity of the perturbed flow is expanded about the base flow as:

$$\mu\,(\boldsymbol{U}_b + \epsilon\,\boldsymbol{u}') = \mu_b + \epsilon\,\mu' + ..., \tag{19}$$

where

$$\mu' = \left.\frac{\partial \mu}{\partial \dot{\gamma}_{ij}}\right|_b \dot{\gamma}_{ij}\,(\mathbf{u}')\ . \tag{20}$$

The deviatoric stresses in the disturbed flow can also be written as:

$$\tau_{ij}\,(\boldsymbol{U}_b + \epsilon\,\boldsymbol{u}') = \tau_{ij}\,(\boldsymbol{U}_b) + \epsilon\tau'_{ij} + ..., \tag{21}$$

with

$$\tau'_{ij} = \mu_b\,\dot{\gamma}_{ij}\,(\boldsymbol{u}') + \mu'\,\dot{\gamma}_{rz}\,(\boldsymbol{U}_b) \tag{22}$$

For one dimensional shear flow, with $W_b(r)$ in the streamwise direction z, the components of the deviatoric stress perturbation read:

$$\tau'_{ij} = \frac{1}{Re}\,\mu_b\,\dot{\gamma}_{ij}\,(\boldsymbol{u}') \quad \text{if} \quad ij \neq rz, zr, \tag{23}$$

$$\tau'_{rz} = \frac{1}{Re}\left[\mu_b + \dot{\gamma}_{rz}\,(\boldsymbol{U}_b)\left.\frac{\partial \mu}{\partial \dot{\gamma}_{rz}}\right|_b\right]\dot{\gamma}_{rz}\,(\boldsymbol{u}') = \frac{1}{Re}\,\mu_t\dot{\gamma}_{rz}\,(\boldsymbol{u}')\,. \tag{24}$$

In Eq. (24), μ_t is the tangent viscosity [14], defined by:

$$\mu_t = (\partial\tau_{rz}/\partial\dot{\gamma}_{rz})_b = n\ |DW_b|^{n-1}\,. \tag{25}$$

It is worthy to note that: (i) μ_t is independent of Hb, i.e. the disturbance "will not feel" the yield stress, and (ii) the deviatoric stress associated to the perturbation is anisotropic. The second invariant of the deviatoric of the stress tensor is linearly disturbed: $|\tau\,(\boldsymbol{U}_b + \epsilon\boldsymbol{u}') - \tau\,(\boldsymbol{U}_b + \epsilon\boldsymbol{u})| = O\,(\epsilon)$. Therefore, the yield surface position r_y is linearly disturbed from its position r_0:

$$r_y = r_0 + \epsilon\,h\,(\theta, z, t)\,. \tag{26}$$

The disturbance is assumed periodic in the z and θ-directions:

$$(u', v', w', p', h') = [u(r,t), v(r,t), w(r,t), p(r,t), h(t)] \exp i(\alpha z + m\theta), \tag{27}$$

where α and m are the axial and azimuthal wave numbers respectively. After some algebra, it can be shown that the linearization of continuity and momentum equations around the base flow leads to the following initial value problem:

$$D(ru) + i[m\,v + \alpha\, r\, w] = 0, \tag{28}$$

$$\begin{aligned}
\frac{\partial u}{\partial t} =& -i\alpha W_b\, u - Dp + \frac{1}{Re}\mu_b\left[\Delta u - \frac{2im}{r^2}v - \frac{u}{r^2}\right] \\
&+ \frac{2}{Re}D\mu\, Du + \frac{i\alpha}{Re}(\mu_t - \mu_b)(Dw + i\alpha u), \qquad (29)\\
\frac{\partial v}{\partial t} =& -i\alpha W_b\, v - \frac{imp}{r} + \frac{1}{Re}\mu_b\left[\Delta v + \frac{2im}{r^2}u - \frac{v}{r^2}\right] \\
&+ \frac{1}{Re}D\mu_b\left(Dv + \frac{i\,m}{r}u - \frac{v}{r}\right), \qquad (30)\\
\frac{\partial w}{\partial t} =& -i\alpha W_b\, w - DW_b u - i\alpha\, p + \frac{1}{Re}\mu_b\,\Delta w \\
&+ \frac{1}{Re}D\mu_b(Dw + i\alpha u) + \frac{1}{Re}\frac{1}{r}\,D\left[r(\mu_t - \mu_b)(Dw + i\,\alpha\, u)\right], \qquad (31)
\end{aligned}$$

with $\Delta \equiv D^2 + \frac{1}{r}D - \frac{m^2}{r^2} - \alpha^2$ and $D \equiv \frac{d}{dr}$. The boundary conditions for the perturbation velocity are obtained from the non-slip and non-penetration at the wall ($r = 1$):

$$u(1) = v(1) = w(1) = 0. \tag{32}$$

The continuity of stress at the yield surface requires

$$\dot{\gamma}_{ij}(\boldsymbol{U}_b + \epsilon \boldsymbol{u}') = 0 \quad \text{at} \quad r = r_y \tag{33}$$

Expanding and linearizing about $r = r_0$ give:

$$u(r_0) = v(r_0) = w(r_0) = 0\,, \tag{34}$$

$$Du(r_0) = Dv(r_0) = 0; \quad Dw(r_0) = \begin{cases} 0 & if \quad n < 1 \\ h\dfrac{2}{(1-r_0)^2} & if \quad n = 1 \end{cases}. \tag{35}$$

We end up with nine boundary conditions: three at the wall and six at the yield surface. The system seems overdetermined. Actually, the conditions

$Du(r_0) = Dv(r_0) = 0$ and $Dw(r_0) = 0$ when $n < 1$ are needed to overcome the singularity in the viscosity at $r = r_0$. When $n = 1$, the boundary condition (35) is a condition for h not for w. The system of equations (28) - (31) may be expressed in terms of u and v if $\alpha \neq 0$ or in terms of u and w if $m \neq 0$. One has to note that at the leading order, the unyielded zone is not disturbed and behaves as a rigid solid from kinematic point of view.

5 Long-time behaviour of the disturbance: eigenvalue problem

When the long time behavior is sought, the disturbance is assumed to behave exponentially as:

$$\mathbf{\Psi}(r,t) = \boldsymbol{\psi}(r) \exp\left(-i\, C\, t\right), \tag{36}$$

where $\mathbf{\Psi}$ stands for $(u,v)^T$ or $(u,\, w)^T$ and $C = C_r + iC_i$ is the complex frequency. The phase speed of the perturbation is given by C_r/α and the growth rate by C_i. The initial value problem is transformed into the following generalized eigenvalue with C as eigenvalue

$$\mathcal{L}_{uv}\,(u,v)^T = C\mathcal{M}_{uv}\,(u,v)^T \quad \text{or} \quad \mathcal{L}_{uw}\,(u,w)^T = C\mathcal{M}_{uw}\,(u,w)^T \tag{37}$$

depending on whether the (u,v) (if $\alpha \neq 0$) or (u,w) (if $m \neq 0$) formulation is used. Note that the eigenvalue problem (37) is only defined on the yielded zone $r \in [r_0,\, 1]$. With increasing the Herschel-Bulkley number, the width $(1-r_0)$ of the sheared fluid zone decreases. To take into account this geometrical effect, the following reduced parameters are introduced:

$$r = \tilde{r}(1-r_0) + r_0,\ z = \tilde{z}(1-r_0),\ t = \tilde{t}(1-r_0), \tag{38}$$

$$\tilde{\alpha} = \alpha\ (1-r_0)\,,\ \tilde{C} = C\ (1-r_0)\,, \tag{39}$$

$$\tilde{Re} = Re\ (1-r_0)^n\,,\ \tilde{Hb} = Hb\ (1-r_0)^n\,. \tag{40}$$

In terms of $\tilde{r}$, the basic velocity profile

$$W_b = 1 - \tilde{r}^{\frac{1+n}{n}} \quad ; \quad \tilde{r} \in [0,1] \tag{41}$$

is artificially independent of the Herschel-Bulkley number. The differential eigenvalue problem (37), written in terms of tilde variables, with the boundary conditions, is discretized using the Chebyshev spectral collocation method [7] at $(N+1)$ Gauss-Lobatto collocation points. The resulting generalized eigenvalue problem is solved using the QZ-algorithm available in Matlab software

package. Spectra with increasing collocation points were compared to determine the adequate number of Chebyshev polynomials $(N+1)$. It was found that with $N = 120$, the first 15 eigenvalues taken by increasing $\tilde{C}_i$ were resolved accurately within four digits (invariant four digits with increasing N) for almost all the situations considered in this paper.

5.1 Case of a one-dimensional perturbation

In the case of a one-dimensional perturbation, i.e. $\tilde{\alpha} = m = 0$, the linear inertial terms which ensure the exchange of energy between the base flow and the perturbation vanish. The initial value problem (28)-(31) with the associated boundary conditions (32)-(35) reduces to

$$u = 0, \qquad p(r) = constant, \tag{42}$$

$$\frac{\partial v}{\partial \tilde{t}} = \frac{1}{\tilde{R}e}\,\frac{1}{\eta^2}\tilde{D}\left(\eta^3\tilde{\mu}_b\tilde{D}\left(\frac{v}{\eta}\right)\right), \tag{43}$$

$$\frac{\partial w}{\partial \tilde{t}} = \frac{1}{\tilde{R}e}\,\frac{1}{\eta}\tilde{D}\left(\eta\tilde{\mu}_t\tilde{D}w\right), \tag{44}$$

where

$$\eta = \tilde{r} + \frac{r_0}{1-r_0},\ \tilde{D} = \frac{d}{d\tilde{r}},\ \tilde{\mu}_b = \frac{\tilde{H}b}{|\tilde{D}W_b|} + |\tilde{D}W_b|^{n-1},\ \tilde{\mu}_t = n\,\tilde{D}|W_b|^{n-1} \tag{45}$$

The boundary conditions are:

$$v(\tilde{r}=1) = w(\tilde{r}=1) = v(\tilde{r}=0) = w(\tilde{r}=0) = 0; \tag{46}$$

Multiplying (30) by v and (31) by w and then integrating from 0 to 1, the following expressions are obtained:

$$\frac{1}{2}\frac{\partial}{\partial \tilde{t}}\left\langle v^2\right\rangle_{\tilde{r}} = -\frac{1}{\tilde{R}e}\left\langle \tilde{\mu}_b\left(\eta\tilde{D}\left(\frac{v}{\eta}\right)\right)^2\right\rangle_{\tilde{r}} \tag{47}$$

and

$$\frac{1}{2}\frac{\partial}{\partial \tilde{t}}\left\langle w^2\right\rangle_{\tilde{r}} = -\frac{1}{\tilde{R}e}\left\langle \eta\,\tilde{\mu}_t\left(\tilde{D}w\right)^2\right\rangle_{\tilde{r}}. \tag{48}$$

where, $\langle(.)\rangle_{\tilde{r}} = \displaystyle\int_0^1 (.)\eta\, d\tilde{r}$.
It is clear that the kinetic energy of the perturbation decreases uniformly

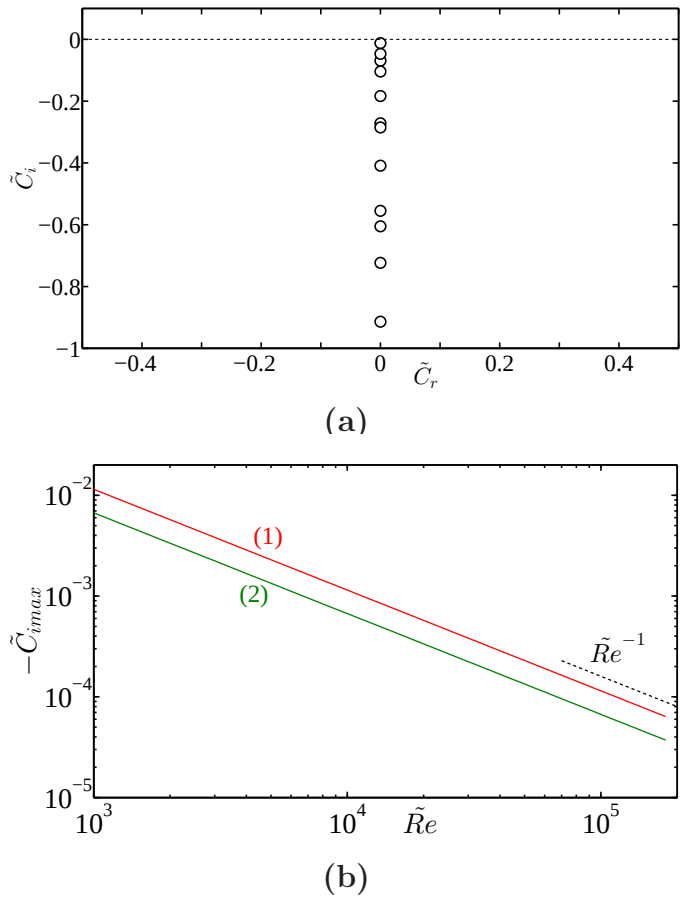

Fig. 3. **(a)** Eigenvalue spectrum for a pipe flow of Herschel-Bulkley fluid at $\tilde{R}e = 5 \times 10^3$, $n = 0.5$, $r_0 = 0.5$, $\tilde{\alpha} = 0$ and $m = 0$. **(b)** Maximum growth rate $\left|\tilde{C}_{i,max}\right|$ vs $\tilde{R}e$ for two different values of shear-thinning index: (1) $n = 1$ and (2) $n = 0.3$

with time. Consequently the Hagen-Poiseuille flow of Herschel-Bulkley fluid is unconditionally linearly stable with respect to one dimensional perturbation. Looking for a solution of (43),(44) as $\exp\left(-i\,\tilde{C}\,t\right)(\hat{v},\hat{w})$, it can be shown straightforwardly that the eigenvalues are purely imaginary. Fig. 3(a) is an example of spectrum obtained at $\tilde{R}e = 5000$ for Herschel-Bulkley fluid with $r_0 = 0.5$ and $n = 0.5$. The maximum growth rate $\tilde{C}_{i,max}$ behaves as $\tilde{R}e^{-1}$ (Fig. 3(b)). For a fixed r_0, $\left|\tilde{C}_{i,max}\right|$ decreases with increasing shear-thinning effects, whereas for fixed n, $\left|\tilde{C}_{i,max}\right|$ increases with increasing r_0. Opposite effects can be found by using a Reynolds number defined with the wall shear-viscosity. The selection of the viscosity scale may be considered a matter of choice, however the conclusion that one reaches by comparing shear-thinning fluids among themselves and against Newtonian fluid can be radically different from one choice to another.

5.2 Case of axisymmetric perturbation: $m = 0$

The (u, v) formulation is used. The differential eigenvalue problem (37) reduces to two decoupled differential equations: the Orr-Sommerfeld and Squire equations.

- The Orr-Sommerfeld modes are solution of the equation

$$\mathcal{L}_{os} u = -i\tilde{C}\tilde{R}eLu, \tag{49}$$

with the boundary conditions:

$$u(1) = \tilde{D}u(1) = u(0) = \tilde{D}u(0) = 0, \tag{50}$$

where, $L \equiv \tilde{D}\tilde{D}^{+} - \tilde{\alpha}^2$, $\tilde{D}^{+} = \tilde{D} + 1/\eta$ and $\mathcal{L}_{os}$ is the Orr-Sommerfeld operator:

$$\begin{aligned}\mathcal{L}_{os} \equiv & -i\tilde{\alpha}\tilde{R}eW_b\, L - i\tilde{\alpha}\tilde{R}e\left(\frac{\tilde{D}W_b}{\eta} - \tilde{D}^2 W_b\right) + \tilde{\mu}_b L^2 + \left(\tilde{D}\tilde{\mu}_b\right)\left(2\tilde{D}L + \frac{1}{\eta}L\right) \\ & + \left(\tilde{D}^2\tilde{\mu}_b\right)\left(L + 2\tilde{\alpha}^2\right) + \left(L + 2\tilde{\alpha}^2\right)\left[\left(\tilde{\mu}_t - \tilde{\mu}_b\right)\left(L + 2\tilde{\alpha}^2\right)\right].\end{aligned} \tag{51}$$

The eigenvalues spectrum of $\tilde{C}$ arising from the discretized operator $-(i/Re)L^{-1}\mathcal{L}_{os}$ exhibits a similar three-branches as for the case of the Newtonian plane Poiseuille flow.

In order to highlight separately the influence of r_0, *i.e,* the modification of the flow geometry on the eigenvalue spectra, we have fixed $n = 1$ and we have canceled artificially $\tilde{H}b$ terms in $\tilde{\mu}_b$ expression. The result is illustrated in Fig. 4(a). For a fixed $\tilde{R}e$, the maximum growth rate increases with decreasing the width of the yielded zone. This result may be related qualitatively with that of Newtonian fluid flow stability in an annular space. In such case, Mott and Joseph [20] have shown that the critical Reynolds number decreases as the ratio of the inner cylinder to that of the outer one increases and approaches 1. In Fig. 4(b), the eigenvalue spectrum obtained for $\tilde{R}e = 5\times10^3$, $\tilde{\alpha} = 1$, $m = 0$, $n = 0.5$, $r_0 = 0.8$ and $\tilde{H}b = 6.9282$ is compared with that obtained by neglecting the $\tilde{H}b$ terms in the Orr-Sommerfeld equation. As it can be observed, there is practically no effect of Hb terms on wall modes. For an axisymmetric perturbation, the wall modes are more sensitive to $\tilde{\mu}_t$ rather than $\tilde{\mu}_b$. Indeed, in Eq. (51), $\tilde{\mu}_t$ terms involve a fourth derivative $\tilde{D}^4 v$, while $\tilde{\mu}_b$ involve a second derivative $\tilde{D}^2 v$. Hence, the wall modes do not "fill" the yield stress.
The influence of the shear-thinning index on the wall modes is illustrated by

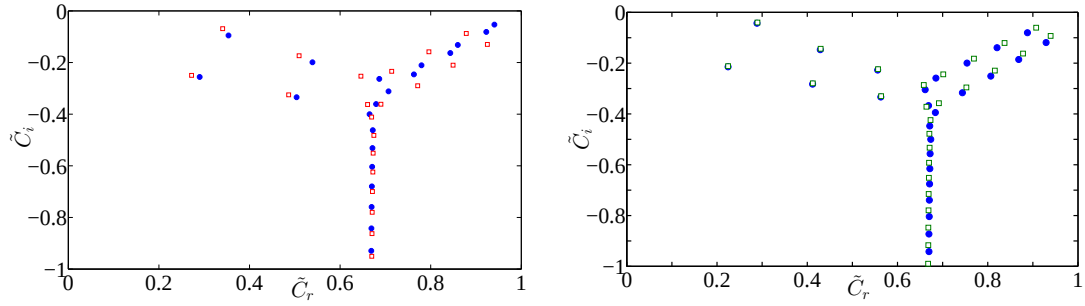

Fig. 4. Modified Orr-Sommerfeld spectra for Herschel-Bulkley fluid flow in a pipe at $\tilde{Re} = 5 \times 10^3$, $\tilde{\alpha} = 1$ and $m = 0$. **(a)** $n = 1$ and the Hb terms are canceled artificially to highlight the influence of r_0: (•) $r_0 = 0.01$ and (□) $r_0 = 0.8$. **(b)** Influence of Hb terms: (•) $r_0 = 0.8$, $\tilde{Hb} = 0.96$; (□) $r_0 = 0.8$, $\tilde{Hb}$ terms neglected

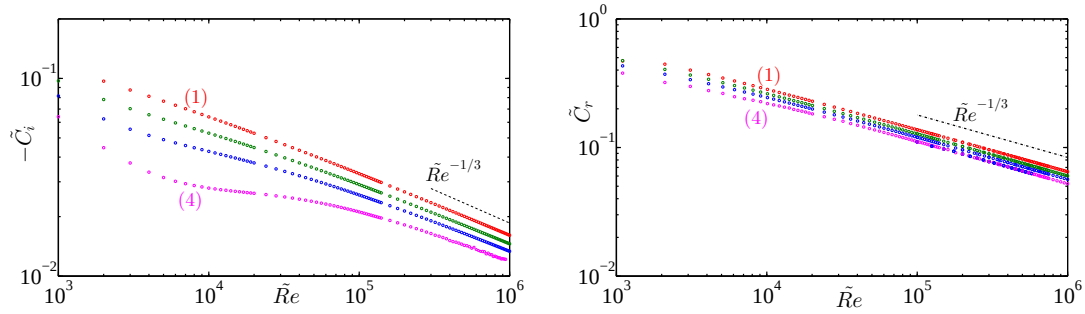

Fig. 5. Herschel-Bulkley fluid flow at $\tilde{Re} = 5000$, with $r_0 = 0.5$, $\tilde{\alpha} = 1$ and $m = 0$. **(a)** Growth rate of the least stable wall mode as function of $\tilde{Re}$: (1) $n = 1$; (2) $n = 0.7$; (3) $n = 5$; (4) $n = 0.3$. **(b)** Phase speed of the least stable mode as function of $\tilde{Re}$: (1) $n = 1$; (2) $n = 0.7$; (3) $n = 5$; (4) $n = 0.3$.

Fig. 5. We have represented $|C_{i,max}|$ and $\tilde{C}_{r,max}$ of the least stable mode, vs $\tilde{Re}$ for different values of n. As n decreases, the viscosity around the plug zone becomes larger and the wall mode is squeezed against the wall. The phase velocity decreases and the growth rate comes closer to the unstable half plane. For large values of $\tilde{Re}$, the scaling with $\tilde{Re}$ is the same as for a Newtonian fluid. Similarly, for interface and mean modes, the scaling with $\tilde{Re}$ is the same as for a Newtonian fluid.

- The Squire modes are solution of the equation

$$\tilde{\alpha} W_b v + i \frac{\tilde{\mu}_b}{\tilde{Re}} \left(\tilde{D}\tilde{D}^+ - \tilde{\alpha}^2 \right) + i \frac{\tilde{D}\mu_b}{\tilde{Re}} \left(\tilde{D} - \frac{1}{\eta} \right) v = \tilde{C} v. \tag{52}$$

with

$$v(0) = v(1) = 0. \tag{53}$$

Multiplying (52) by v^*, where the star designates the complex conjugate, and integrating between the yield surface and the wall gives:

$$\tilde{C}_i \left\langle |v|^2 \right\rangle_{\tilde{r}} = -\left\langle \frac{\tilde{\mu}_b}{\tilde{R}e} \left[\tilde{\alpha}^2 |v|^2 + \left| \tilde{D}v - \frac{v}{\eta} \right|^2 \right] \right\rangle_{\tilde{r}}, \tag{54}$$

It is clear that the Squire modes are always damped.

5.3 Case of streamwise homogeneous perturbation: $\tilde{\alpha} = 0$ and $m \neq 0$

The $(u,\, w)$ formulation is used. On setting $\tilde{\alpha} = 0$, the eigenvalue problem (37) reduces to

$$\begin{aligned} i\tilde{C}\left[\left(\tilde{D}^+u\right)^2 + \frac{1}{\eta}\tilde{D}^+u - \frac{m^2}{\eta^2}u\right] &= -\frac{\tilde{\mu}_b}{\tilde{R}e}\left[\left(\tilde{D}^+u\right)^2 + \frac{1}{\eta}\tilde{D}^+u - \frac{m^2}{\eta^2}u\right]^2 \\ &\quad -\tilde{D}\tilde{\mu}_b\tilde{R}e\left[\left(\frac{1}{\eta}\tilde{D}\tilde{D}^+u + 2\tilde{D}^3u + \frac{4\tilde{D}^2}{\eta}u - \frac{2m^2}{\eta^2}\tilde{D}u + \frac{m^2}{\eta^3}u\right)\right] \\ &\quad -\frac{\tilde{D}^2\tilde{\mu}_b}{\tilde{R}e}\left[\tilde{D}\tilde{D}^+u - \frac{m^2}{\eta^2}u\right] \end{aligned} \tag{55}$$

$$\begin{aligned} -i\tilde{C}w = -\tilde{D}W_\ell u + \frac{\tilde{\mu}_b}{\tilde{R}e}\left[\frac{1}{\eta}\tilde{D}\left(\eta\tilde{D}w\right) - \frac{m^2}{\eta^2}w\right] \\ +\frac{\tilde{D}\tilde{\mu}_b}{\tilde{R}e}\tilde{D}w + \frac{1}{\eta}\tilde{D}\left[\eta\left(\tilde{\mu}_t - \tilde{\mu}_b\right)\left(\tilde{D}w\right)\right] \end{aligned} \tag{56}$$

The set of eigenvalues of the system (55) and (56) can be divided into two eigenmodes classes. The first one corresponds to the set of the eigenmodes of (55) with a particular solution of (56). The second class represents the set of eigenmodes of (56) with $u = 0$. It can be shown straightforwardly that the eigenmodes are always damped. They are pure imaginary, i.e. the eigenmodes do not propagate and decrease monotonically with time. An example of the eigenvalues spectrum for $\alpha = 0$, $m = 1, \tilde{R}e = 5000$, $n = 0.5$ and $r_0 = 0.5$ is shown in Fig. 6(a). The eigenvalues cluster to the origin with increasing $\tilde{R}e$. For the streamwise case $m = 1$ and $\alpha = 0$, the maximum growth rate approaches zero as $\tilde{R}e \to \infty$ almost exactly as $\tilde{R}e^{-1}$. Figure 6(b) displays the variation of $\left|\tilde{C}_i\right|_{max}$ as a function of $\tilde{R}e$ for two different values of the shear-thinning

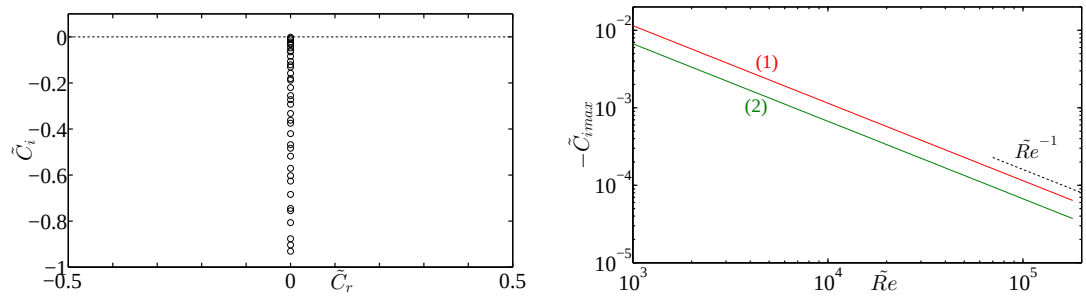

(a) **(b)**

Fig. 6. **(a)** Eigenvalue spectrum at $\tilde{Re} = 5 \times 10^3$, $\tilde{\alpha} = 0$, $m = 1$, $n = 0.5$ and $r_0 = 0.5$. **(b)** Evolution of the maximum growth rate as a function of $\tilde{Re}$ for $n = 1$, curve (1) and $n = 0.3$, curve (2).

index. The numerical results indicate that $\tilde{C}_{i,max}$ decreases with decreasing n.

Remark: Comparison with the situation of annular Poiseuille flow with sliding inner cylinder

In the linear theory, the unyielded zone behaves as a rigid solid moving axially with a constant velocity. The Hagen-Poiseuille flow of a yield stress fluid can be viewed a priori as a combined axial Poiseuille Couette flow of a shear-thinning fluid in a cylindrical annulus. To our knowledge, this problem has not been considered before in the literature. For a Newtonian fluid, Sadeghi and Higgins[21] studied the stability of sliding Couette-Poiseuille flow in an annulus to both axisymmetric and asymmetric perturbations. Computations were performed for a radius ratio $R_1/R_2 = 0.5$ and $0 \leq m \leq 3$. Preziosi and Rosso [22] studied the linear stability of a Newtonian fluid between sliding pipes. The linearized disturbance equations were solved numerically for a radius ratio $R_1/R_2 \geq 0.1$, $\alpha \leq 10$ and $m \leq 5$ and a Reynolds number, based on the axial velocity of the moving cylinder, less than 10^4. For this range of parameters, the authors did not observe any instability. Gitler [23], using a long-wave version of the axisymmetric Orr-Sommerfeld equation (proposed initially by Cowley and Smith [24]), showed that for a radius ratio $R_1/R_2 < 0.1415$, the Couette flow is linearly unstable from a finite Reynolds number. Based on Gitler's results, one might expect that Hagen-Poiseuille flow of a yield stress fluid would be unstable at a finite critical Reynolds number at least for $r_0 \leq 0.14$. A long wave-approximation of the Orr-Sommerfeld equation for Herschel-Bulkley was established (see Appendix A) and solved numerically for two values of r_0 : 0.1 and 0.05. We have not found any instability. This is probably due to the fact that the velocity profile can not be written as the sum of Couette and Poiseuille flow of a yield stress fluid.

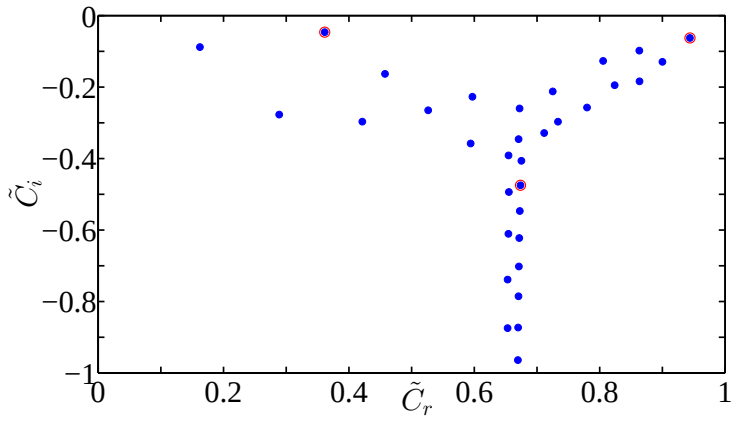

Fig. 7. Eigenvalues distribution at $\tilde{\alpha} = 1$, $m = 1$, $\tilde{Re} = 5 \times 10^3$, $r_0 = 0.1$ and $n = 0.5$.

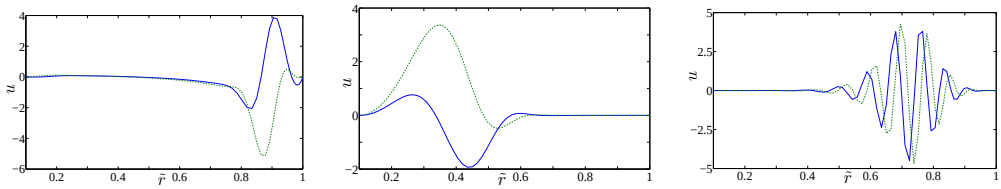

(a) **(b)** **(c)**

Fig. 8. Eigenfunctions at $\tilde{Re} = 5000$, $n = 0.5$, $r_0 = 0.1$ with $\tilde{\alpha} = m = 1$. **(a)** Wall mode ; **(b)** interfacial mode; **(c)** mean mode. Continuous line is the real part and dashed line is the imaginary part.

5.4 Case of oblique perturbation : $\tilde{\alpha} \neq 0$ and $m \neq 0$

In this situation, either the (u, v) or the (u, w) formulation can be used. The shape of the eigenvalue spectrum is similar to that of a Newtonian fluid, except that for a yield stress fluids, there are two separate vertical branches, one of them is associated to the Squire modes described in §5.2 as shown in figure 7. As an indication, we have represented the eigenfunctions u for the three selected eigenmodes. As expected, for the wall eigenmode, variations of the axial velocity occur mainly near the wall, while for the interfacial eigenmode, variations are observed near the yield surface (interface). The mean mode is mainly characterized by oscillations in the associated eigenfunctions.

Finally for the range of the rheological parameters considered in this study, all the eigenmodes lie in the stable half of the complex plane. Thus, it is conjectured that Poiseuille flow of Herschel-Bulkley fluid in a cylindrical pipe is linearly stable with respect to infinitesimal perturbations.

6 Short time behavior: pseudospectra, transient growth and optimal perturbation

6.1 Nonnormality: pseudospectra and numerical range

The eigenvalues describe the time asymptotic behavior of disturbances. Thus for Hagen-Poiseuile flow of yield stress fluids, a perturbation introduced at $t = 0$ decays to zero for large times. The stability analysis based on eigenvalues is not sufficient to describe the temporal behavior of the disturbance at all times because of the non-normality of the linear operator. This mathematical property means that there is a potential for extraction of energy from the base flow by a subspace of perturbation leading to transient growth, despite the absence of an exponential instability.
The non-normality of the linear stability operator $\mathcal{L} \equiv \mathcal{M}^{-1}_{uw(uv)}\mathcal{L}_{uw(uv)}$, Eq. (37), is characterized by using ϵ-pseudospectrum and numerical range tools (Trefethen *et al.* [25], Reddy *et al.* [26], Schmid & Henningson [27]). The computation needs to define an inner product and a norm.
For a velocity disturbance vector-function $\boldsymbol{q} = (u, v)^T$, the scalar product based on the energy density is defined as

$$(\boldsymbol{q}_1, \boldsymbol{q}_2)_E = \int_{r_0}^{1} \boldsymbol{q}_2^H Q \boldsymbol{q_1} r \mathrm{d}r \quad \text{with} \tag{57}$$
$$\boldsymbol{q}_2^H Q \boldsymbol{q_1} = u_1 u_2^* + \frac{1}{\alpha^2} D^+ u_1 D^+ u_2^* + \left(1 + \frac{m^2}{\alpha^2 r}\right) v_1 v_2^* + \frac{im}{\alpha^2 r}\left(v_1 D^+ u_2^* - D^+ u_1 v_2^*\right),$$

where the superscript 'H' means transpose conjugate. The associated energy norm is given by

$$||\boldsymbol{q}||_E = (\boldsymbol{q}, \boldsymbol{q})_E = \int_{r_0}^{1} \boldsymbol{q}^H Q \boldsymbol{q} r \mathrm{d}r. \tag{58}$$

Q is a positive definite matrix. It can be decomposed into $Q = F^H F$ using a Cholesky decomposition. The energy norm of a perturbation is equivalent to the standard (Eucledian)$L2$-norm of the vector $F\boldsymbol{q}$.
Let $\mathcal{F}$ be the discrete representation of $\mathcal{L}$. The ϵ-pseudospectrum of $\mathcal{F}$ is defined as the set of complex numbers z for which $||\left(z\mathcal{I} - \mathcal{F}\right)^{-1}||_E \geq \epsilon^{-1}$. It is usually displayed graphically with contours of the norm of the resolvent $(z\mathcal{I} - \mathcal{F})^{-1}$ for various values of ϵ. Pseudospectra can also be defined as the set of complex numbers z which are eigenvalues of $\mathcal{F} + \Delta\mathcal{F}$ for some perturbation matrix $\Delta\mathcal{F}$ with $||\Delta\mathcal{F}||_E \leq \epsilon$. The more non-normal the linear operator $\mathcal{L}$, the greater the potential for a disturbance operator $\Delta\mathcal{F}$ to affect the eigenvalues. A third equivalent definition of the ϵ-pseudospectrum, closer to computation,

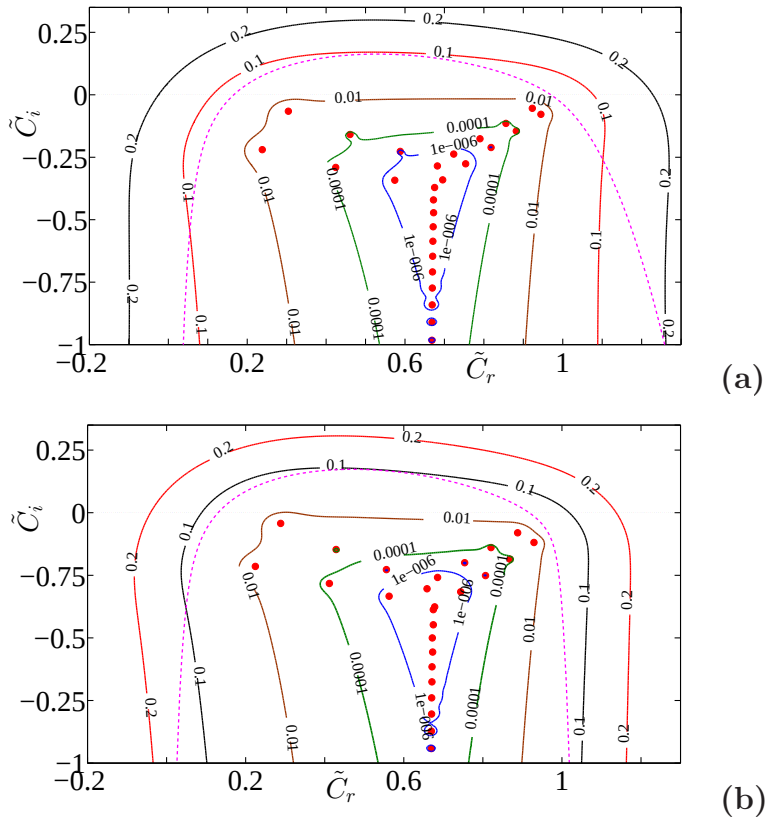

Fig. 9. Spectral portrait of the modified Orr-Sommerfeld operator at $\tilde{Re} = 5000$, $\tilde{\alpha} = 1$, for a Herschel-Bulkley fluid: influence of the radius plug zone. Continuous lines are the boundaries of the ϵ-pseudospectra and the dashed line is the numerical range. **(a)** $n = 0.5$, $r_0 = 0.01\,(\tilde{Hb} = 0.017)$, **(b)** $n = 0.5$, $r_0 = 0.8\,(\tilde{Hb} = 6.93)$.

involves the singular value decomposition. It is the set of complex numbers z for which $\sigma_{min}\left(z\mathcal{I} - F\mathcal{F}F^{-1}\right) \leq \epsilon$, where σ_{min} is the smallest singular value. The numerical range of $\mathcal{F}$ is the set of complex numbers $(\mathcal{F}\mathbf{q}, \mathbf{q})_E / (\mathbf{q}, \mathbf{q})_E$. For a normal operator, the numerical range is the convex hull of the spectrum. Therefore, for a stable normal operator, the numerical range is always in the stable half plane. However, it can extend significantly to even protrude into the unstable half plane for stable non-normal operators. Its maximum protrusion determines the maximum energy growth rate at $t = 0^+$ ([28], [29])

6.1.1 Axisymmetric perturbation

In figure 9, spectra, pseudospectra and numerical ranges of the linear stability operator $\mathcal{L}_{os}$ (51) are shown for axisymmetric perturbations with $\tilde{\alpha} = 1$, $n = 0.5$, $\tilde{Re} = 5000$ and two values of the plug radius $r_0 = 0.01$ and 0.8. It is clear that the Orr-Sommerfeld operator is non-normal. At $\tilde{Re} = 5000$, perturbations with norm $\epsilon > 0.01$ is necessary to protrude the pseudospectra in the unstable half plane. As expected for axisymmetric perturbations, the influence of r_0

or $\tilde{H}b$ on the pseudospectra is very weak. Indeed, the perturbation is mainly sensitive to the tangent viscosity which is independent of the yield stress.

6.1.2 streamwise homogeneous perturbation

Spectra, pseudospectra and numerical ranges of the linear stability operator (55), (56) for streamwise homogeneous perturbation (longitudinal rolls) are depicted in Figure 10 at $\tilde{R}e = 5000$, $\tilde{\alpha} = 0$, $m = 1$, $n = 0.5$ and two values of r_0: 0.01 ($\tilde{H}b = 0.017$) and 0.8 ($\tilde{H}b = 6.93$). On contrast with the former case, the increase of $\tilde{H}b$ reduces significantly the extension of the pesudospectra in the unstable half plane. For instance, at $r_0 = 0.01$, a perturbation of norm $\epsilon \approx 5.2 \times 10^{-6}$ is necessary to reach the unstable half plane, while for $r_0 = 0.8$, a much more intense perturbation $\epsilon \approx 1.0 \times 10^{-3}$ is needed.

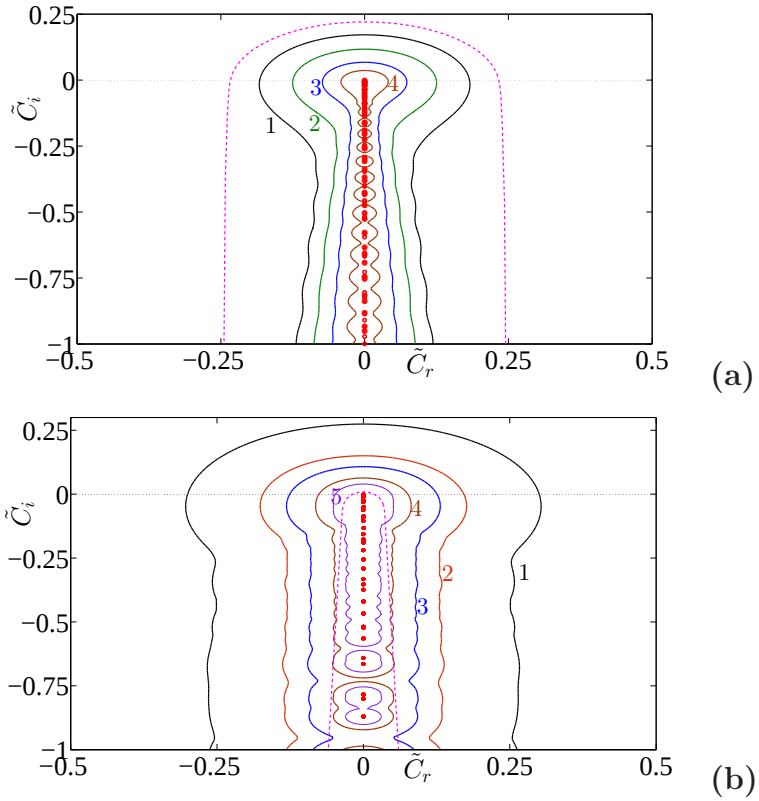

Fig. 10. Spectral portrait of the linear operator for streamwise homogeneous perturbation at $\tilde{R}e = 5000$, $n = 0.5$, $\tilde{\alpha} = 0$ and $m = 1$. The dashed curve is the numerical range of the linear operator considered. Continuous line curves delimit the isovalues of the ϵ-pseudospectra. **(a)** $r_0 = 0.01$: (1) $\epsilon = 2.5 \times 10^{-3}$, (2) $\epsilon = 1.5 \times 10^{-3}$, (3) $\epsilon = 7 \times 10^{-4}$, (4) $\epsilon = 3 \times 10^{-4}$; **(b)** $r_0 = 0.8$: (1) $\epsilon = 0.25$, (2) $\epsilon = 0.13$, (3) $\epsilon = 9 \times 10^{-2}$, (4) $\epsilon = 5 \times 10^{-2}$, (5) $\epsilon = 3 \times 10^{-2}$

6.1.3 *Oblique perturbation*

For an oblique perturbation, the pseudospectra and numerical ranges are qualitatively similar to those obtained for an axisymmetric perturbation. However, the influence of $\tilde{H}b$ is much more significant. Increasing $\tilde{H}b$ reduces the maximum protrusion of the numerical range and the extension of the pseudospectra in the unstable half plane.

6.1.4 *Norm of the minimal perturbation*

As for Newtonian fluids, the norm of the minimal destabilizing perturbation, ϵ_{min} behaves as $(\tilde{Re}^{-1/2})$ for large $\tilde{Re}$. Note that for a given $\tilde{Re}$, ϵ_{min} decreases with decreasing n or r_0.

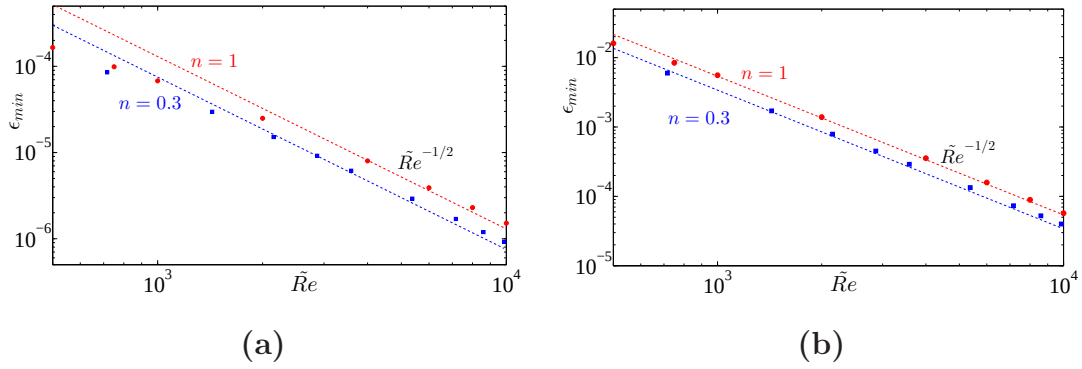

Fig. 11. Norm of the minimal destabilizing perturbation as a function of the modified Reynolds number for two values of the shear-thinning index, $n = 0.1$ and 0.3 and two values of r_0: **(a)** $r_0 = 0.01$; **(b)** $r_0 = 0.8$. The axial and azimuthal wavenumbers are $\tilde{\alpha} = 1$ and $m = 1$ respectively.)

6.2 *Transient growth and optimal disturbances*

The transient evolution of perturbations in the linear regime is determined following the methodology described by Schmid and Henningson [27]. Let $g(t)$ the ratio between the energy norm $||\boldsymbol{q}(t)||_E$ of the perturbation at time t and its initial norm $||\boldsymbol{q}_0||_E$

$$g(t) = \frac{||\boldsymbol{q}(t)||_E}{||\boldsymbol{q}_0||_E} \tag{59}$$

For a given Fourier mode, the amplification of the energy at time t maximized over all possible non-zero initial conditions is denoted by

$$G(t, \alpha, m) = \sup_{\boldsymbol{q}_0 \neq 0} g(t). \tag{60}$$

The maximum transient energy growth possible over all times is

$$G_{max}(\alpha, m) = \sup_{t} G(t, \alpha, m). \tag{61}$$

The maximum of G_{max} for all the pairs (α, m) is

$$G^{opt} = \sup_{\alpha, m} G(\alpha, m), \tag{62}$$

which is reached by the optimal perturbation at time t^{opt}. Unlike the modal approach, here the growth of disturbances occurs over relatively short initial time and is related to an inviscid mechanism. The viscosity acts to moderate the amplification.

6.2.1 Transient growth for a given Fourier mode

- Case of oblique and streamwise homogeneous perturbations

Figure 12 shows the kinetic energy amplification $G(\tilde{t})$ as a function of time at $\tilde{Re} = 3000$ and three values of the dimensionless yield stress: $\tilde{Hb} = 0.02\,(r_0 = 0.01)$, $\tilde{Hb} = 0.22\,(r_0 = 0.1)$, $\tilde{Hb} = 0.5\,(r_0 = 0.2)$. The flow behavior index n is fixed to $n = 1$. Two different initial conditions are considered: longitudinal rolls with $\tilde{\alpha} = 0$, $m = 1$ (Fig. 12a) and oblique perturbation $\tilde{\alpha} = 1$, $m = 1$ (Fig. 12b). With increasing $\tilde{Hb}$, the viscosity increases thus reducing the viscous diffusion time and therefore t_{max} and G_{max}. At very low $\tilde{Hb}$, the transient growth remains significantly lower than that obtained for a Newtonian fluid, particularly for the case of $\tilde{\alpha} = 0$, $m = 1$. The unmatched transient growth at the limit $\tilde{Hb} = 0$ is explained as follows. In the framework of the linear stability analysis, it is assumed that the perturbation is infinitesimal with respect to all scales of the base flow. If ϵ is a characteristic scale of the perturbation size, therefore $\epsilon = o(r_0)$. In other words, the yield surface is linearly disturbed and the plug zone remains intact ([17], [30]). Hence, when the Hb terms are canceled artificially in the perturbation equations, one recovers the linear stability problem of Couette-Poiseuille flow between two coaxial cylinder where the outer is fixed and the inner is moving with a constant axial velocity $W = 1$.

- Case of axisymmetric perturbations

For axisymmetric perturbations, the influence of r_0 on the transient growth is relatively weak. Indeed, for an axisymmetric perturbation, spectra, pseudospectra and numerical range do not substantially depend on r_0.

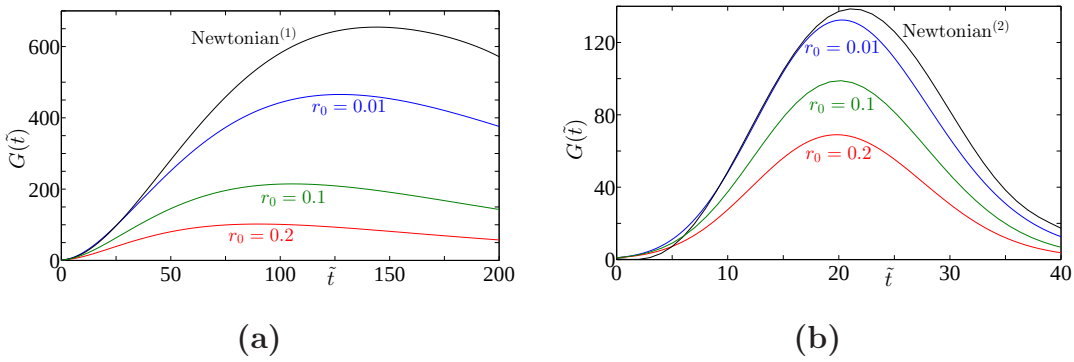

Fig. 12. kinetic energy amplification at $\tilde{Re} = 3000$, $n = 1$ and different values of the plug radius r_0: $r_0 = 0.01$ ($\tilde{Hb} = 0.02$), $r_0 = 0.1$ ($\tilde{Hb} = 0.22$) and $r_0 = 0.2$ ($\tilde{Hb} = 0.5$). **(a)** $\tilde{\alpha} = 0$, $m = 1$. The Newtonian curve is given by Schmid and Henningson [27]. **(b)** $\tilde{\alpha} = 1$, $m = 1$. The Newtonian curve is given by Meseguer and Trefethen [31].

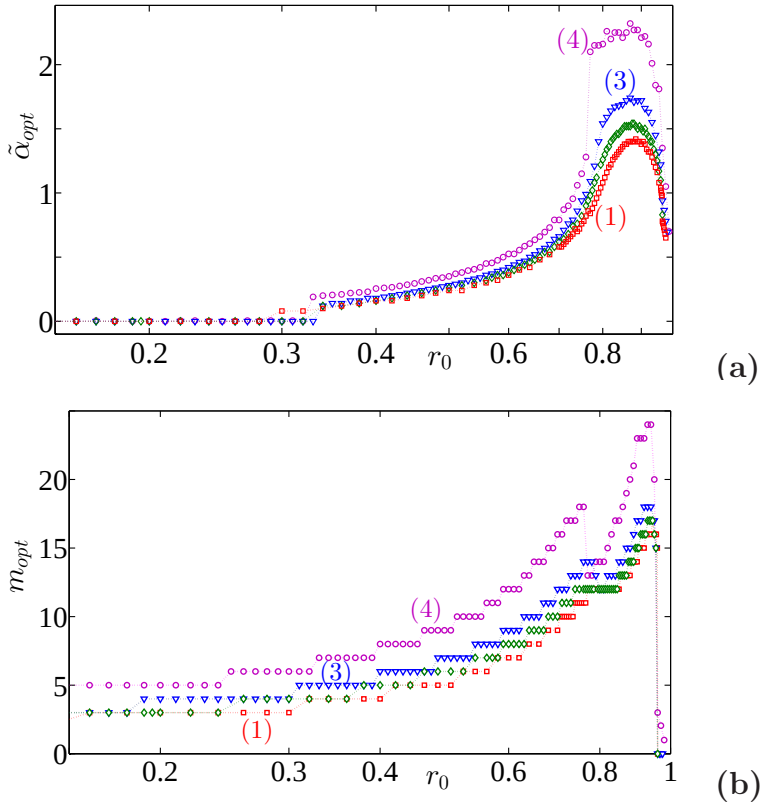

Fig. 13. Optimal axial wavenumber $\tilde{\alpha}_{opt}$ **(a)** and optimal azimuthal wavenumber m_{opt} **(b)** as a function of the radius of the plug zone at $\tilde{Re} = 5000$ and for three values of the shear-thinning index: (1) $n = 1$, (2) $n = 0.7$, (3) $n = 0.5$ and $n = 0.3$.

6.2.2 Characteristics of the optimal perturbation and optimal transient growth

We have computed G^{max} at $\tilde{Re} = 5000$ and for the set of rheological parameters $n = 0.3$, 0.5, 0.7 and 1, with $0.001 \leq r_0 \leq 0.96$ ($0.0017 \leq \tilde{Hb} \leq 48.0$). The characteristics of the optimal perturbations, i.e. $\tilde{\alpha}_{opt}$ and m_{opt} corresponding

to $\max_{\tilde{\alpha},m}(G^{max})$ are displayed in the Figure 13 as a function of the plug zone radius. Three regions can be distinguished depending mainly on r_0:

(i) The first region holds for low values of r_0, say $r_0 \lesssim 0.33$, which corresponds to $\tilde{Hb} \leq 0.74$ when $n = 0.5$. In this region, $\alpha_{opt} = 0$ and the optimal azimuthal wavenumber m_{opt} increases with increasing shear-thinning effects. The optimal perturbation consists of pairs of counter-rotating streamwise vortices, In Figure 14, we have represented the structure of the optimal perturbation at $t = 0$ and $\tilde{t} = \tilde{t}_{opt}$ for $r_0 = 0.01$ and $n = 0.5$. These streamwise counter-rotating vortices allow the transfer of energy to the streamwise-velocity component by the lift-up mechanism creating high (+) and low (−) streamwise streaks displayed in Fig. 14(b). Note that the location of the maximum streamwise velocity component approaches the wall with increasing $\tilde{Hb}$ or r_0. At $t = 0$, almost all the energy is in the azimuthal (61.52%) and radial (38.46%) components and only a negligible part is in the streamwise component. At optimal time, $t = t^{opt}$, the kinetic energy is merely concentrated in the axial component.
(ii) The second region holds for $0.35 \lesssim r_0 \lesssim 0.93$. In this region, $\tilde{\alpha}_{opt}$ increases gradually until $\tilde{\alpha} \approx 0.5$ at $r_0 \approx 0.6$, then strongly until a maximum at $r_0 \approx 0.93$. With increasing $\tilde{Hb}$ or shear-thinning effects, the width of the zone where the exchange of energy between the base flow and the perturbation occurs, is reduced leading to an increase of m_{opt}. The optimal perturbation is oblique and its wave vector has an angle which increases with increasing r_0. The time evolution of the axial velocity component, in the (r, z) and (r, θ) planes is shown in Fig. 15. The optimal perturbation is initially oriented in the direction opposite to the mean shear, then aligned with it at the optimal time. As indicated by Farrell and Ioannou [6], the kinetic energy of the perturbation is amplified thanks to Orr- and lift-up mechanisms. An alternative explanation of the transient growth was proposed by Vitoshkin *et al.* [32]. These authors pointed out the role played by the interplay between the spanwise (here azimuthal) vorticity q and the divergence plane d (in the shear-plane, rz). This is highlighted in the analysis of the energy growth via the Reynolds stress production term. For this, a 2D Helmoltz decomposition is performed:

$$\boldsymbol{u} = \boldsymbol{u}_d + \boldsymbol{u}_q \quad \text{with} \quad \boldsymbol{u}_d = \boldsymbol{\nabla}(\varphi) \quad \text{and} \quad \boldsymbol{u}_q = -\boldsymbol{rot}(\psi \boldsymbol{e}_\theta), \tag{63}$$

where φ and ψ are scalar functions such that the planar divergence $d = \partial u/\partial r + u/r + \partial w/\partial z$ and the azimuthal vorticity $q = \partial v/\partial r + v/r - (1/r)\partial u/\partial \theta$ satisfy

$$d = \Delta_H(\varphi) \quad \text{and} \quad q = \Delta_H(\psi) \tag{64}$$

where $\Delta_H \equiv \partial^2/\partial r^2 + (1/r)\partial/\partial r + \partial^2/\partial z^2$ is the 2D Laplacian in the shear plane (r, z). The energy growth via the Reynolds stress is

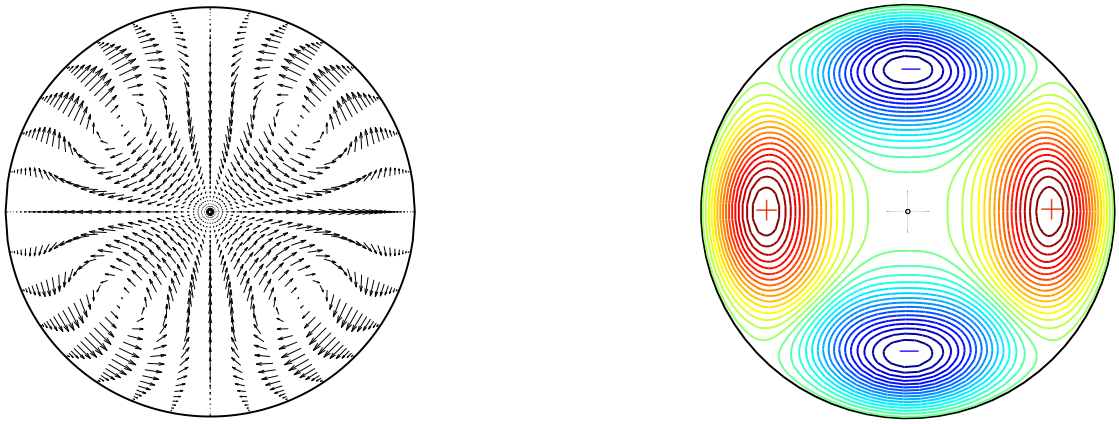

(a) **(b)**

Fig. 14. Optimal perturbation and optimal streaks at $\tilde{Re} = 5000$, $n = 0.5$, $r_0 = 0.01$ ($\tilde{Hb} = 0.0175$): $\alpha = 0$ and $m = 2$. **(a)** Velocity vectors $u\boldsymbol{e_r} + v\boldsymbol{e_\theta}$ of the optimal perturbation at $t = 0$. **(b)** Axial velocity w contours at $t = t^{opt} = 165$

$$\begin{aligned}\frac{\partial \langle E \rangle}{\partial t} &= -\Re\left\langle \dot{\gamma}^b_{rz} u w^* \right\rangle \\ &= -\Re\left\langle \dot{\gamma}^b_{rz} \left(u_d + u_q\right)\left(w^*_d + w^*_q\right)\right\rangle \\ &= -\Re\left\langle \dot{\gamma}^b_{rz} u_d\, w^*_d\right\rangle - \Re\left\langle \dot{\gamma}^b_{rz} u_q\, w^*_q\right\rangle - \Re\left\langle \dot{\gamma}^b_{rz} u_d\, w^*_q\right\rangle - \Re\left\langle \dot{\gamma}^b_{rz} u_q\, w^*_d\right\rangle,\end{aligned} \tag{65}$$

with $E = |\boldsymbol{u}|^2$ and $\langle(\cdot)\rangle = \int_{r_0}^{1}(\cdot) r dr$. Time evolution of the different terms is depicted in Fig. 16(a) for $n = 0.5$, $r_0 = 0.5$, $\tilde{Re} = 5000$. The first term on the right-hand side of Eq. (65) represents the contribution of the planar divergence to the energy growth. This contribution is positive, but relatively small. The second term, i.e. the rotational term $-\left\langle \dot{\gamma}^b_{rz} u_q w^*_q \right\rangle$, is the contribution of the 2D Orr-mechanism. Initially, this term is positive and participates to the increase of E. From $t = t_{opt}/2$, the vortices are tilted with the shear and $-\left\langle \dot{\gamma}^b_{rz} u_q w^*_q \right\rangle$ is negative: the Orr-mechanism contributes to the decay of the energy. The third term, $-\left\langle \dot{\gamma}^b_{rz} u_d w^*_q \right\rangle$ is the first mixed $q-d$ term. It is positive and contributes strongly to the energy growth and is able to overwhelm the large negative contribution of the Orr-mechanism, when the vortices align with the base shear. The fourth term, $-\left\langle \dot{\gamma}^b_{rz} u_q w^*_d \right\rangle$ is the second mixed $q-d$ term. It is small and negative. With increasing r_0, the contribution of the Orr-mechanism in the amplification of the perturbation kinetic energy becomes more significant as illustrated in Fig. 16(b) and 16(c).

(iii) For very large plug radius, $0.93 \leq r_0 < 1$, the optimal perturbation is axisymmetric. The transient growth of the perturbation energy arises from the Orr-mechanism. It is associated with the tilting of the disturbance into the direction of the mean shear. This tilting phenomenon is illustrated by Fig.

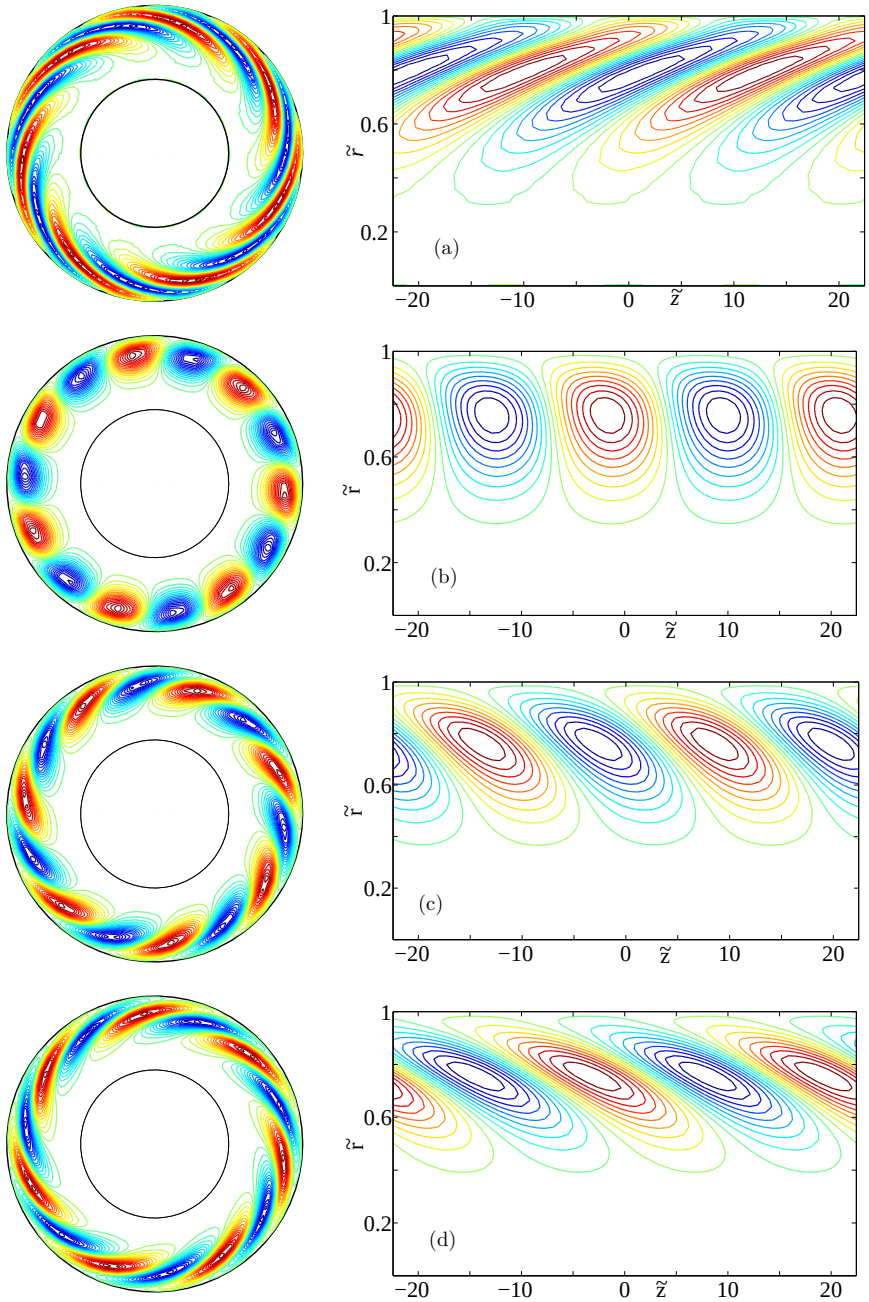

Fig. 15. Temporal evolution of the optimal perturbation. $n = 0.5$, $r_0 = 0.5\,(\tilde{Hb} = 1.732)$, $\tilde{Re} = 5000$, with $\tilde{\alpha}_{opt} = 0.28$, $m_{opt} = 7$, $\tilde{t}_{opt} = 38.6$. Axial velocity contours at **(a)** $\tilde{t} = 0$; **(b)** $\tilde{t} = \tilde{t}_{opt}/2$; **(c)** $\tilde{t} = \tilde{t}_{opt}$; **(d)** $\tilde{t} = (3/2)\tilde{t}_{opt}$.

17, where contours of axial velocity of the optimal perturbation are displayed at different times. In contrast with the previous situation (ii), the 2D optimal perturbation is oriented transversally to the main shear at the optimal time.

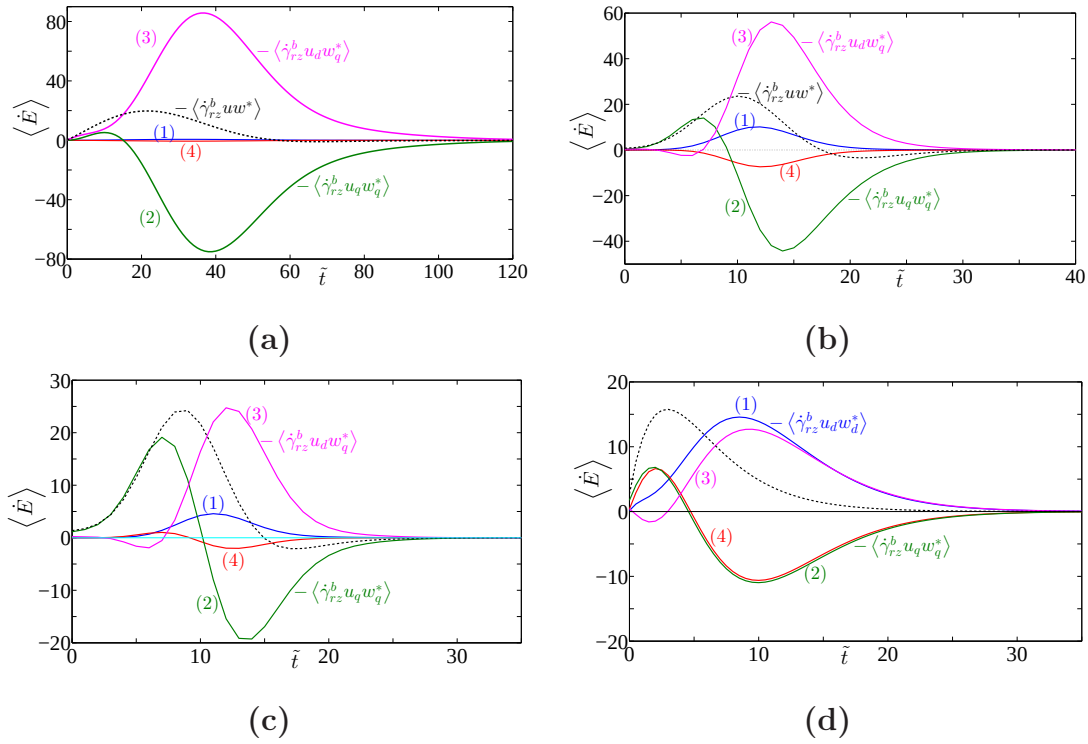

Fig. 16. Contribution of the different Reynolds-stress components to the energy amplification for an optimal oblique perturbation at $\tilde{Re} = 5000$, with **(a)** $n = 0.5$, $r_0 = 0.5$, $\tilde{\alpha} = 0.28$, $m = 7$; **(b)** $n = 0.5$, $r_0 = 0.8$, $\tilde{\alpha} = 1.54$, $m = 12$; **(c)** $n = 0.5$, $r_0 = 0.9$, $\tilde{\alpha} = 1.715, m = 17$; **(d)** Case where $\mu_t - \mu_b$ terms and their derivatives are canceled, $n = 0.5$, $r_0 = 0.9, \tilde{\alpha} = 0.6, m = 44$. (1) $-\langle \dot{\gamma}_{rz} u_d w^*_d \rangle$; (2) $-\langle \dot{\gamma}_{rz} u_q w^*_q \rangle$; (3) $-\langle \dot{\gamma}_{rz} u_d w^*_q \rangle$; (4) $-\langle \dot{\gamma}_{rz} u_q w^*_d \rangle$

6.2.3 Discussion

- If we set $n = 1$, and we cancel artificially $\tilde{Hb}$ terms in the linear stability operators, we recover the Couette-Poiseuille flow of a Newtonian fluid. The optimal perturbation consists of longitudinal counter rotating vortices pairs ($\alpha = 0$) for any $r_0 < 1$. The lift-up mechanism is the only operating mechanism in the energy amplification. The azimuthal wavenumber increases significantly with increasing r_0. A slight increase of G_{opt} with increasing r_0 is observed.
- The obliquity of the optimal perturbation which may be characterized by the ratio $arctang(\alpha/m)$ is a consequence of the anisotropy terms, i.e. terms arising from the viscosity perturbation. Indeed, if we cancel artificially $\mu_t - \mu_b$ terms as well as their derivatives, the obliquity is strongly reduced. For instance at $r_0 = 0.9$, the ratio α/m is much small (10 times smaller) when the anisotropy terms are neglected. Note that the energy amplification is also significantly reduced and the lift-up is the main mechanism operating. The contribution of the different terms of Eq. (65) in the transient growth at $r_0 = 0.9$ and $n = 0.5$ is represented in Fig. 16(d). Comparatively to Fig. 16(c), the contribution of the Orr mechanism is limited.

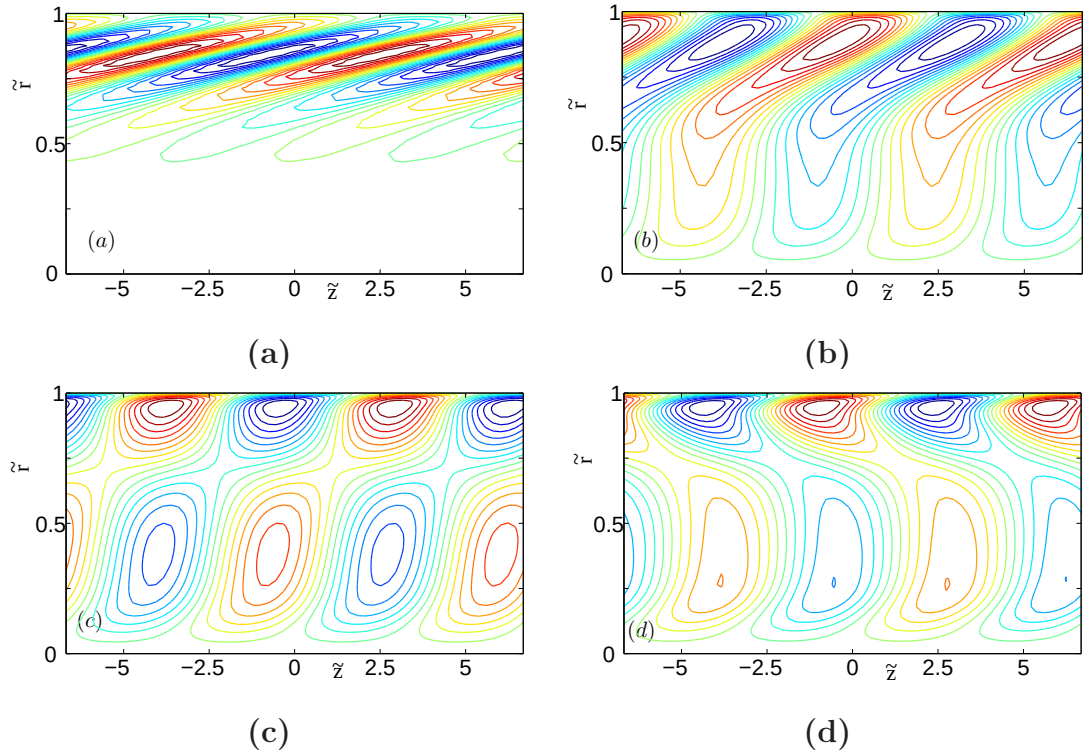

Fig. 17. Temporal evolution of the optimal perturbation. $n = 0.5$, $r_0 = 0.96\,(\tilde{Hb} = 41.47)$, $\tilde{Re} = 5000$, with $\tilde{\alpha}_{opt} = 0.94$, $m_{opt} = 0$, $\tilde{t}_{opt} = 16.2$. Axial velocity contours at **(a)** $\tilde{t} = 0$; **(b)** $\tilde{t} = \tilde{t}_{opt}/2$; **(c)** $\tilde{t} = \tilde{t}_{opt}$; **(d)** $\tilde{t} = (3/2)\tilde{t}_{opt}$.

6.2.4 Scaling laws for G_{opt} and t_{opt}

For given r_0 and n, the dependence of G^{opt} and t^{opt} on Re is studied. It is found that G^{opt} increases with $\tilde{Re}$. The scaling with Re^2, Fig 18(a) is recovered for Hershel-Bulkley fluids in the first region where $\alpha = 0$. It also applies in the second region until $r_0 \lesssim 0.6$, where the lift-up mechanism is the dominant mechanism in the transient growth (Fig. 16(a)). Similarly, the scaling of t^{opt} with Re is satisfied, Fig. 18(b). Analysis of the numerical results show that they can be fitted as

$$\frac{G_{opt}}{\tilde{Re}^2} = A_n \exp\left(B_n\, r_0\right) \quad \text{and} \quad \frac{\tilde{t}_{opt}}{\tilde{Re}} = A'_n \exp\left(B'_n\, r_0\right)\,, \tag{66}$$

where the coefficients A_n, $A'n$ and the exponents B_n, depend on n. They are given in Table 1

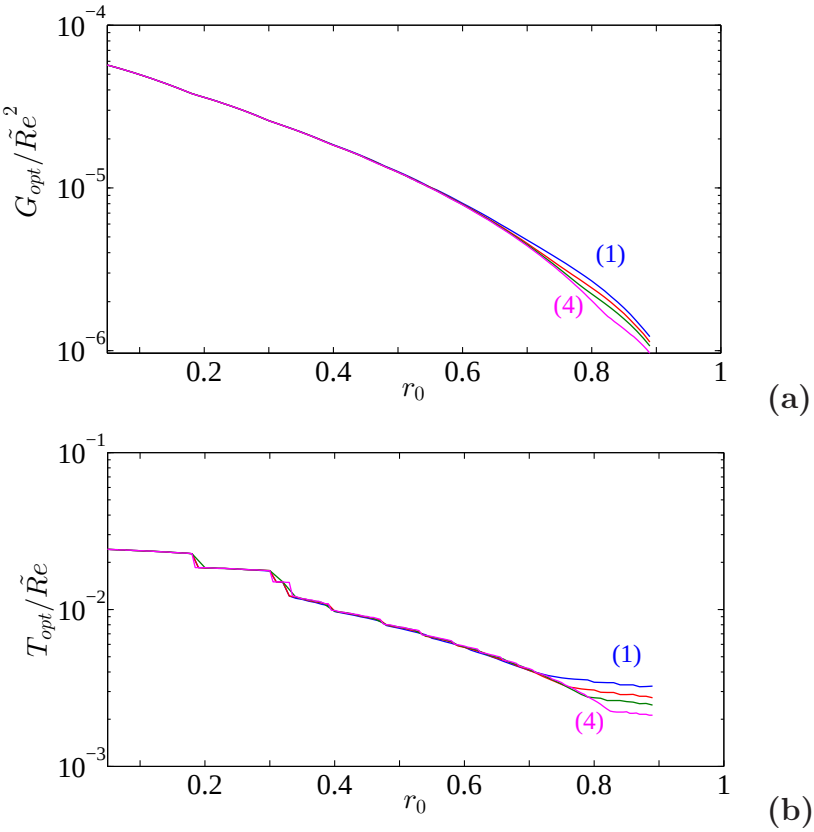

Fig. 18. Variation of $G_{opt}/\tilde{Re}^2$ and $T_{opt}/\tilde{Re}$ as a function of the radius of the plug zone for $n = 0.5$ and different values of the $\tilde{Re}$: (1) $Re = 3000$, (2) $\tilde{Re} = 4000$, (3) $\tilde{Re} = 5000$, (4) $\tilde{Re} = 7000$.

n	0.3	0.5	0.7	1
$A_n \times 10^6$	66.1	68.1	68.1	62.9
B_n	-2.22	-3.28	-3.55	-3.62
$A'_n \times 10^3$	24.6	32.1	35.4	32.9
B'_n	-2.72	-2.81	-2.96	-2.8

Table 1
Fitting coefficients in the scaling laws $G_{opt}/\tilde{Re}^2$ and $t_{opt}/\tilde{Re}$ for different values of the shear-thinning index n.

7 Energy stability, Euler-Lagrange equations

In this section, the maximum Reynolds number, Re_{cE}, below which, the perturbation kinetic energy decreases monotonically with time is determined. In the yielded zone, $\Omega = [0; 2\,\pi]\times]r_0; 1] \times [0; 2\pi/\alpha]$, the mean kinetic energy, E, of a three dimensional perturbation is defined by:

$$E = \frac{1}{||\Omega||} \int_{\Omega} \left[\frac{u'^2_r + v'^2_r + w'^2_r}{2} \right] d\Omega, \tag{67}$$

where u'_r is the real part of $u(r,t)\, exp\,[i(\alpha\, z + m\theta)]$ and similarly for v'_r and w'_r. Hence, E can be written as

$$E = \frac{1}{2\,(1 - r_0^2)} \int_{r_0}^{1} \left[u\, u^* + v v^* + w w^* \right] r\, dr \tag{68}$$

The temporal variation of the mean kinetic energy $\dfrac{dE}{dt}$ is obtained by multiplying the linearized perturbation equations (29), (30) and (31) by u^*, v^* and w^* respectively and then integrated over the domain Ω, with the condition $\boldsymbol{u} = 0$ at the wall and at the interface. The result is a modified Reynolds-Orr equation, which after some algebra, is given by

$$\left(1 - r_0^2\right) \frac{dE}{dt} = \mathcal{I}\,(\boldsymbol{u}) - \frac{1}{Re} \left[\mathcal{V}(\boldsymbol{u}) - \mathcal{A}(\boldsymbol{u}) \right] \tag{69}$$

where $\mathcal{I}\,(\boldsymbol{u})$, $\mathcal{V}(\boldsymbol{u})$ and $\mathcal{A}(\boldsymbol{u})$ denote the inertial, viscous and anisotropy terms, defined by

$$\mathcal{I}(\boldsymbol{u}) = -\left\langle DW_b \left(u_r w_r + u_i w_i \right) \right\rangle, \tag{70}$$

$$\mathcal{V}(\boldsymbol{u}) = \left\langle \mu_b \left(|D\boldsymbol{u}|^2 + \left(\alpha^2 + \frac{m^2}{r^2} \right) |\boldsymbol{u}|^2 + \frac{|u|^2 + |v|^2}{r^2} - \frac{2im}{r^2} \left(u v^* - u^* v \right) \right) \right\rangle, \tag{71}$$

$$\mathcal{A}(\boldsymbol{u}) = \left\langle \left(\mu_b - \mu_t \right) |Dw + i\alpha u|^2 \right\rangle. \tag{72}$$

In the above equations $|u|^2 = u_r^2 + u_i^2$, $|\boldsymbol{u}|^2 = |u|^2 + |v|^2 + |w|^2$ and $\langle (.) \rangle = \displaystyle\int_{r_0}^{1} (.) r\, dr$. There is no energy growth of the perturbation, i.e, the basic flow remains "energy stable", if $\dfrac{dE}{dt} < 0$. Define Re_1 as the largest value of Re for which this condition is satisfied

$$\frac{1}{Re_1} = \max_{\boldsymbol{u}} \frac{I(\boldsymbol{u})}{\mathcal{V}(\boldsymbol{u}) - \mathcal{A}(\boldsymbol{u})}, \tag{73}$$

where $\boldsymbol{u}$ is an admissible perturbation satisfying the continuity equation and the boundary conditions. This constrained optimization problem is solved using variational calculus. The corresponding Euler-Lagrange equations are

$$wDW_b = -D\xi + 2\Lambda\left[\mu_b\left(\triangle u - \frac{2im}{r^2}v - \frac{u}{r^2}\right) + 2\frac{d\mu}{dr}\frac{du}{dr}\right] + 2\Lambda\left[i\alpha\left(\mu_t - \mu_b\right)\left(Dw + i\alpha\right)\right], \quad (74)$$

$$0 = -\frac{im}{r}\xi + 2\Lambda\left[\mu_b\left(\triangle v + \frac{2im}{r^2}u - \frac{v}{r^2}\right) + \frac{d\mu_b}{dr}\left(Dv + \frac{im}{r}u - \frac{v}{r}\right)\right], \quad (75)$$

$$uDW_b = -i\,\alpha\,\xi + 2\Lambda\left[\mu_b \triangle w + \frac{d\mu}{dr}\left(Dw + i\alpha u\right)\right] + 2\Lambda\frac{1}{r}D\left[r\left(\mu_t - \mu_b\right)\left(Dw + i\alpha u\right)\right]. \quad (76)$$

with

$$Du + \frac{u}{r} + i\left[\frac{m}{r}v + \alpha\, w\right] = 0. \quad (77)$$

Equations (74)-(76) define an eigenvalue problem, where Λ is the eigenvalue to compute and

$$Re_1\left(\alpha, m, n, Hb\right) = max\,\Lambda. \quad (78)$$

The eigenvalue problem (74)-(76) is solved numerically using the procedure described in §5 with mapping $[r_0, 1]$ into $[0, 1]$ and the transformations (38) - (40). The results of the numerical computation are presented in terms of marginal stability curves, *i.e.* curves in the $\left(\tilde{\alpha}, \tilde{Re}_1\right)$ plane, that separate regions of initial energy density growth from regions of initial energy decay.

Influence of the plug radius

In order to highlight the influence of the unyielded zone radius, r_0, on the global stability conditions, the $\tilde{Hb}$ terms are canceled artificially and n is fixed to 1. Figure 19 shows in this particular case, i.e. Couette-Poiseuille flow of a Newtonian fluid, that the most dangerous perturbation is a streamwise vortices ($\alpha = 0$) with an azimuthal wavenumber m increasing with r_0. The maximum Reynolds number, $\tilde{Re}_{CE} = \min_{\tilde{\alpha},m} \tilde{Re}_1\left(\tilde{\alpha}, m\right)$, that ensures no energy growth, depends weakly on r_0. When $r_0 \to 1$, $\tilde{Re}_{cE}$ tends towards the value obtained by Nouar *et al.* [17] for a Bingham plane Poiseuille flow, i.e. $\tilde{Re}_{cE} = 79.82$. When $r_0 \to 0$, $\tilde{Re}_{cE}$ tends to $\tilde{Re}_{cE} = 91.08$. This value is different from that obtained by Joseph and Carmi[33] for Hagen-Poiseuille flow of a Newtonian fluid, i.e. $\tilde{Re}_{cE} = 81.49$. This singularity is a consequence of the boundary conditions at the yield surface.

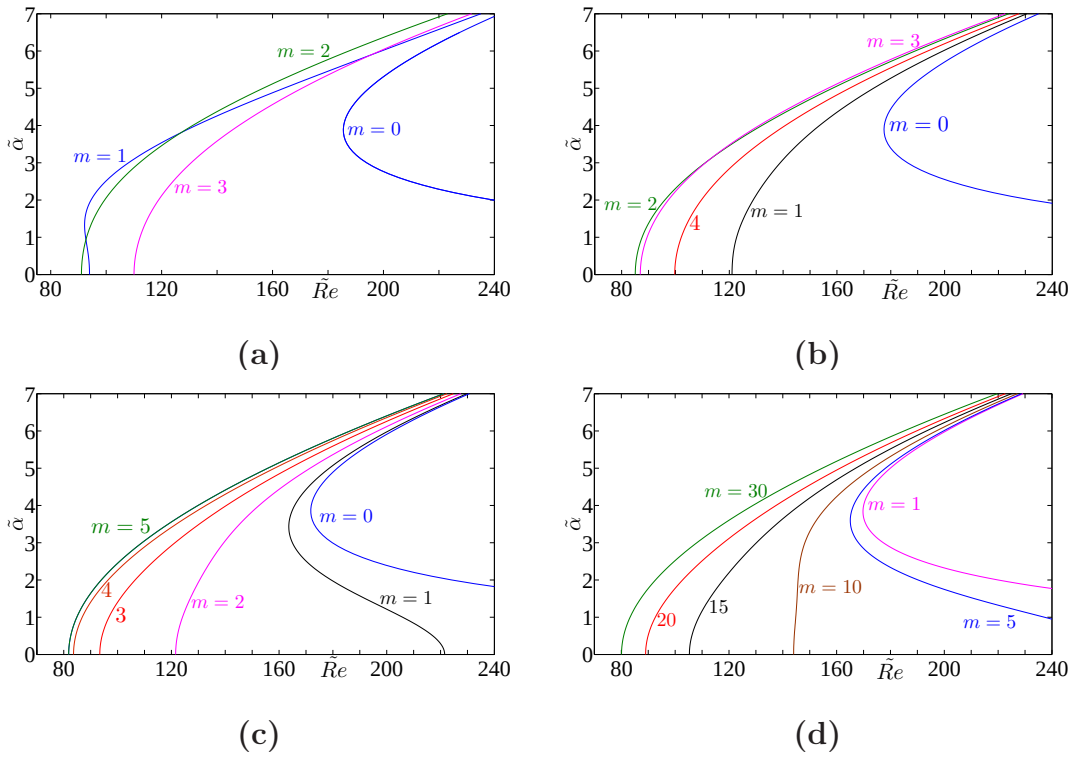

Fig. 19. Newtonian Couette-Poiseuille flow. Boundaries in the $(\tilde{\alpha}, \tilde{Re})$ delimiting zones of global stability. **(a)** $r_0 = 0.001$, $\tilde{Re}_{cE} = 91.08$; **(b)** $r_0 = 0.2$, $\tilde{Re}_{cE} = 85.06$; **(c)** $r_0 = 0.5$, $\tilde{Re}_{cE} = 81.84$; **(d)** $r_0 = 0.9$, $\tilde{Re}_{cE} = 80.06$. The curves are labeled with the azimuthal wavenumber

Viscosity stratification without anisotropy terms

The influence of the viscosity stratification, on the global stability is illustrated in Fig. 20. The terms arising from the viscosity perturbations are canceled. It is worthy to note that: (i) the most dangerous perturbation is a streamwise perturbation with an azimuthal wavenumber m_c larger that obtained for a Newtonian Couette-Poiseuille flow; (ii) the critical Reynolds number Re_{CE} increases strongly with increasing r_0 (or Hb), because of the increase of the viscous dissipation. From $\tilde{Hb} \approx 30$, the numerical results show that $\tilde{Re}_{cE} \propto \tilde{Hb}$.

Viscosity stratification with anisotropy terms

Taking into account the $\tilde{Hb}$ terms with $n < 1$, reduces significantly the critical Reynolds number for no energy growth. For weak values of $\tilde{Hb}$, the critical conditions are still obtained for a perturbation in the form of streamwise vortices but with lower azimuthal wavenumber, 21(a). The variation of $\tilde{Re}_{cE}$ with n is fitted by $\tilde{Re}_{cE} \approx 91.1 - 26(1-n)$, for $0.3 \leq n \leq 1$.
With increasing $\tilde{Hb}$, the most dangerous perturbation becomes oblique 21(b). For sufficiently high value of $\tilde{Hb}$, the critical mode is axisymmetric, as shown in figure (19), where variations of the critical axial $\tilde{\alpha}$ and azimuthal m wavenumbers as function of $\tilde{Hb}$ are represented. It is worth noting that for the ax-

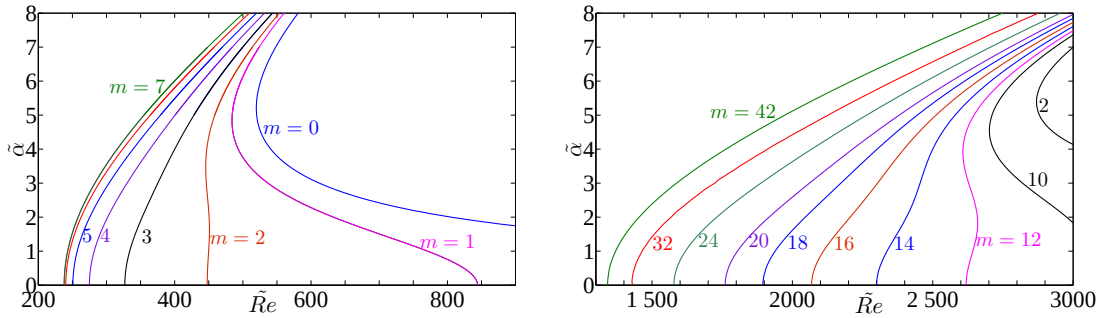

(a) **(b)**

Fig. 20. Influence of viscosity stratification without anisotropy terms. Boundaries in the $(\tilde{\alpha}, \tilde{Re})$ delimiting zones of global stability. **(a)** $r_0 = 0.5, n = 0.5, \tilde{Hb} = 1.73, m_c = 7, \tilde{Re}_{cE} = 237.9$; **(b)** $r_0 = 0.9, \tilde{Hb} = 15.59, m_c = 42, \tilde{Re}_{cE} = 1342$. The curves are labeled by the azimuthal wavenumber.

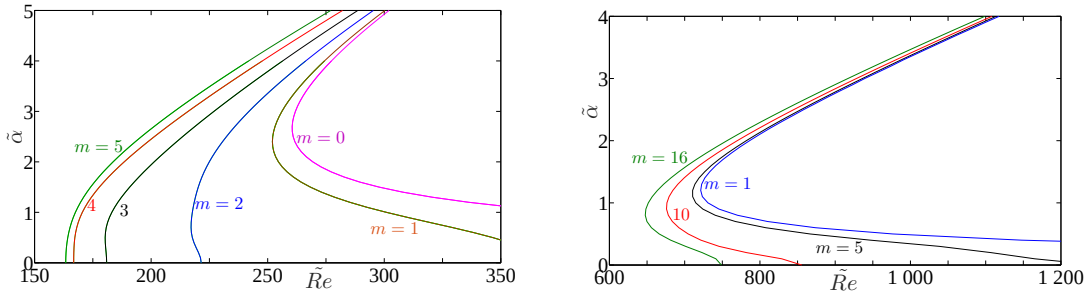

(a) **(b)**

Fig. 21. Viscosity stratification with anisotropy terms. Boundaries in the $(\tilde{\alpha}, \tilde{Re})$ delimiting zones of global stability: Effect of the plug zone width. **(a)** $r_0 = 0.5, n = 0.5, \tilde{Hb} = 1.73, m_c = 5, \tilde{\alpha}_c = 0, \tilde{Re}_{cE} = 163.37$; **(b)** $r_0 = 0.9, n = 0.5, \tilde{Hb} = 15.59, m_c = 16, \tilde{\alpha}_c = 0.8, \tilde{Re}_{cE} = 647.64$.

isymmetric perturbation, the viscous dissipation involves the tangent viscosity $\mu_t < \mu_b$. The variation of the critical Reynolds number, $\tilde{Re}_{CE}$ is given by the curve (1) in figure 23. The conditional stability derived by Nouar and Frigaard [34] for Bingham fluid is also represented by curve (2). In this analysis, the effect of the yield stress is limited to the modification of the unyielded zone radius. For large $\tilde{Hb}$ ($\tilde{Hb} \geq 30$), $\tilde{Re}_{cE}$ varies as $\tilde{Hb}^{1/2}$. The numerical results may be fitted as $\tilde{Re}_{cE} \approx 218 n^{0.46} \tilde{Hb}^{1/2}$. It is interesting to note that for plane Poiseuille flow of a Bingham fluid, it is found $\tilde{Re}_{cE} \approx 217 \tilde{B}^{1/2}$. Concerning the critical wavenumber, the following asymptotic behavior is obtained, $\tilde{\alpha} \sim \tilde{Hb}^{-1/2}$. It can be considered as an extension of the theoretical prediction done by Frigaard and Nouar [35] for a Bingham fluids to Herschel-Bulkley fluids.

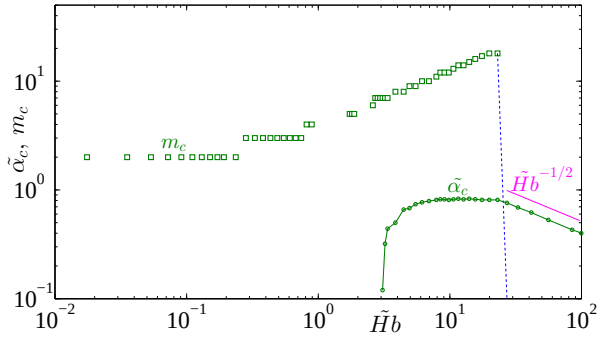

Fig. 22. Evolution of the critical axial and azimuthal wavenumbers ($\tilde{\alpha}_c$ and m_c as function of $\tilde{Hb}$. The shear-thinning index is fixed: $n = 0.5$.

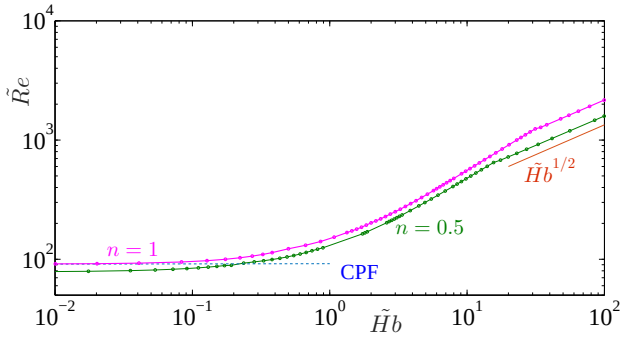

Fig. 23. Critical Reynolds numbers, $\tilde{Re}_{CE}$ versus $\tilde{Hb}$. The shear-thinning index is fixed $n = 0.5$. CPF denotes the limit of a Newtonian Couette-Poiseuille flow between coaxial cylinder when $r_0 \to 0$.

8 Conclusion

Linear stability analysis and receptivity of Hagen-Poiseuille flow of Herschel-Bulkley fluid are investigated using modal and non modal approaches. The base flow is mainly characterized by (i) a central plug zone of radius r_0 moving with a constant velocity and (ii) a nonlinear variation of the viscosity between the wall and the yield surface. Two dimensionless parameters govern the problem: the shear-thinning index n and the modified Herschel-Bulkley number $\tilde{Hb}$ or equivalently n and r_0. In the linear stability analysis, taking into account the viscosity perturbation leads to an anisotropy of the stress-tensor perturbation. The component $\tau'_{rz} = \tau'_{zr}$ involves the tangent viscosity μ_t, which is independent of the yield stress, while the other components τ'_{ij}, $ij \neq rz, zr$ involve the effective viscosity $\mu_b > \mu_t$.
The results of the modal approach show that: (i) In the case of an axisymmetric perturbation, the influence of Hb (dimensionless yield stress) is reduced mainly to the modification of the width of the yielded zone; (ii) In the case of an oblique perturbation, the Hb terms contribute to stabilize the flow through an increase of the viscous dissipation; (iii) The Hagen-Poiseuille flow of Herschel-Bulkley fluid is asymptotically stable to infinitesimal disturbances.

Because of the non-normality of the linear stability operators (with respect to a scalar product based on the energy norm), a transient algebraic amplification of the kinetic energy of the perturbation is observed. The influence of the rheological parameters on the transient growth and the characteristics of the optimal perturbation is studied. It is shown that: (i) with increasing the dimensionless yield stress $\tilde{Hb}$, the amplification of the kinetic energy G_{max} is reduced. However, for an axisymmetric perturbation, $\tilde{Hb}$ has practically no effect on G_{max}. (ii) For $\tilde{Hb} << 1$, the optimal perturbation is in the form of longitudinal rolls. The amplification of the kinetic energy is governed by the lift-up mechanism. The scaling laws in $\tilde{Re}^2$ for G_{opt} and $\tilde{Re}$ for t_{opt} are recovered. (iii) With increasing $\tilde{Hb}$, shear-thinning effects become more significant, the optimal perturbation is oblique in the plane (r, z) with an axial wavenumber $\tilde{\alpha} = O(1)$. The optimal azimuthal wavenumber increases with decreasing the width of the yielded zone. The optimal perturbation evolves by the effects of Orr and Lift-up mechanisms. (iv) For sufficiently large value of $\tilde{Hb}$, the optimal perturbation is axisymmetric and the transient growth occurs only by the Orr-mechanism.
Concerning the energy stability analysis and the determination of the maximum Reynolds number Re_{CE} below which the kinetic energy of the perturbation decreases uniformly with time, the numerical results show that for $\tilde{Hb} << 1$, with $0.3 \leq n \leq 1$, the most dangerous perturbation is in the form of longitudinal rolls with $\tilde{Re}_{cE} \approx 91.1 - 26(1-n)$. For large $\tilde{Hb}$, the most dangerous perturbation is axisymmetric and $Re_{cE} \approx 218 n^{0.46} \tilde{Hb}^{0.5}$, with $\tilde{\alpha} \propto \tilde{Hb}^{-0.5}$. If the viscosity perturbation is not taken into account, $\tilde{Re}_{cE} \propto \tilde{Hb}$.

The different scaling laws, given in sections §6-§7, involve the dimensionless parameters Hb and Re defined with a generalized viscosity, $\hat{\mu}_{gen}$ (§2) derived from the dimensionless form of the momentum equations. However, the structure of: (i) the base flow, the less stable mode and (iii) the optimal perturbation, suggests that wall shear viscosity is a more appropriate choice of viscosity scale. For an axisymmetric perturbation, tangent wall shear viscosity is even more relevant. Results obtained in terms of Re and can be expressed in terms of wall Reynolds number, Re_w, using the relation $Re_w = Re\,(1-r_0)^n\,[n/(n+1)]^{n-1}$. Using Re_w rather than Re does not globally change the conclusions given above. Nevertheless, the comparison of yield-stress shear-thinning fluids among themselves does require to indicate the scale viscosity adopted.

This work puts just a brick to a more comprehensive building to identify possible paths of transition. Experimental studies of transition to turbulence in a pipe for yield stress fluids were performed by Peixinho *et al.* [36], Esmael *et al.* [37] and Guzel *et al.* [38]. A weakly turbulent flow is observed, where the

time-averaged axial velocity profiles exhibit an asymmetry. The mechanism associated to this nonlinear asymmetry is not yet clarified.
The present work can be pursued in two directions. The first one, also based on linear stability equations, starts from the realization that the base flow around which the linearization is performed is just an idealization, whereas in reality small defects inevitably occur. This approach proposed by Bottaro *et al.* [39] has shown some success in capturing features of transition in pipe flow (Gavarinni *et al.* [40], Ben-Dov & Cohen [41], [42]). It was applied for the first time to the channel flow of Bingham flow by Nouar *et al.* [43], where scaling laws for transition were proposed. The second direction, is to determine a weakly nonlinear optimal perturbation. This approach, proposed recently by Pralits *et al.* [44] allows to identify initial states which relaminarize from those which grow without bound.

A Long wave approximation

Following the asymptotic method introduced by Cowley and Smith [24] for a Couette-Poiseuille flow, the following "long-wave" eigenvalue problem is derived for an axisymmetric perturbation:

$$i\lambda\left(W_b-\omega\right)\left(\phi''-\frac{1}{r}\phi'\right)+i\lambda\left(\frac{DW_b}{r}-D^2W_b\right)\phi \tag{A.1}$$

$$=F^{n-1}\left[n\phi'''-\frac{2n}{r}\phi'''+\frac{3n}{r^2}\left(\phi''-\frac{1}{r}\phi'\right)\right] \tag{A.2}$$

$$+\left(n-1\right)F^{n-1}\frac{DF}{F}\left(n\phi'''-\frac{3n}{r}\left(\phi''-\frac{1}{r}\phi'\right)\right) \tag{A.3}$$

$$+n\left(n-1\right)F^{n-1}\left(\left(n-2\right)\frac{\left(DF\right)^2}{F^2}+\frac{D^2F}{F}\right)\left(\phi''-\frac{1}{r}\phi'\right), \tag{A.4}$$

where $\phi=ru$, $\lambda=\tilde{\alpha}\tilde{Re}$, $\omega=\tilde{C}/\tilde{\alpha}$ and $F=|DW_b|$. Equation A.4 is solved by the same method as that described in §5. Figure A.1 shows the evolution of the eigenvalue ω as a function of λ. We have not found any instability.

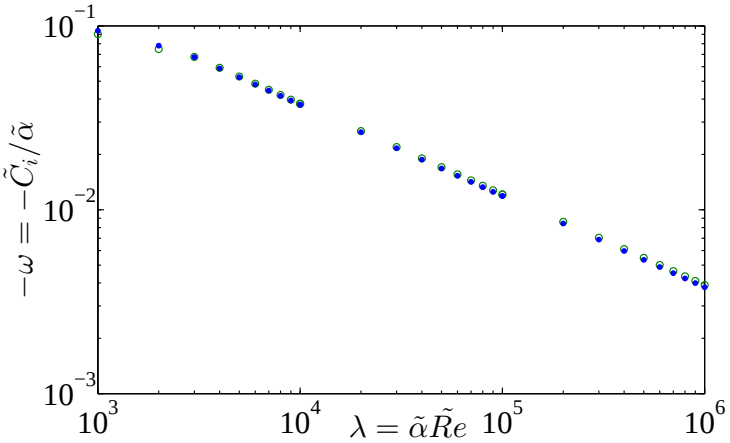

Fig. A.1. Maximum temporal amplification rate of the perturbation as function of $\lambda = \tilde{\alpha}\tilde{R}e$ at $n = 0.5$ and two values of the plug zone radius: (□) $r_0 = 0.8$ and (•) $r_0 = 0.1$.

References

[1] S. Grossmann. The onset of shear flow turbulence. *Rev. Mod. Phys.*, 72:603–618, 2000.

[2] W.M.F. Orr. The stability or instability of the steady motions of a perfect liquid and of a viscous liquid. part I: A perfect liquid. *Proc. R. Irish. Acad. A*, 27:9–68, 1907.

[3] T. Ellingsen and E. Palm. Stability of linear flow. *Phys. Fluids. A*, 18:487–488, 1975.

[4] M. T. Landhall. A note on an algebraic instability of inviscid parallel shear flows. *J. Fluid. Mech.*, 98:243–251, 1980.

[5] K.M. Buttler and B. Farrell. Three optimal perturbations in viscous shear flow. *Phys. Fluids. A*, 4:1637–1650, 1992.

[6] B. Farrell and P.J. Ioannou. Optimal excitation of three-dimensional perturbations in viscous constant shear flows. *Phys. Fluids. A*, 5(6):1390–1400, 1993.

[7] P. J. Schmid and D. S. Henningson. *Stability and transition in shear flows.* Springer - Verlag, New York, 2001.

[8] L. Brandt. The lift-up effect: The linear mechanism behind transition and turbulence in shear flows. *Eur. J. Mech. B-Fluid*, 47:80, 2014.

[9] M.R. Jovanovic and S. Kumar. Transient growth without inertia. *Phys. Fluids.*, 22:023101, 2010.

[10] M.R. Jovanovic and S. Kumar. Nonmodal amplification of stochastic disturbances in strongly elastic channel flows. *J. Non-Newtonian. Fluid Mech.*, 166:755–778, 2011.

[11] M. Zhang, I. Lashgari, T.A. Zaki, and L. Brandt. Linear stability analysis of channel flow of viscoelastic Oldroyd-B and FENE-P fluids. *J. Fluid Mech.*, 737:249–279, 2013.

[12] R. Govindarajan and K.C. Sahu. Instabilities in viscosity-stratified flows. *Annu. Rev. Fluid Mech.*, 46:331–353, 2014.

[13] V. Chikkadi, A. Sameen, and R. Govindarajan. Preventing transition to turbulence: A viscosity stratification does not always help. *Phys. Rev. Lett.*, 95:264504, 2005.

[14] C. Nouar, A. Bottaro, and J.P. Brancher. Delaying transition to turbulence in channel flow: revisiting the stability of shear-thinning fluids. *J. Fluid Mech.*, 592:177–194, 2007.

[15] R. Liu and Q.S. Liu. Nonmodal stability in hagen poiseuille flow of a shear-thinning fluid. *Phys. Rev. E.*, 85:066318, 2012.

[16] R. Liu and Q.S. Liu. Non-modal instability in plane Couette flow of a power-law fluid. *J. Fluid Mech.*, 676:145–171, 2011.

[17] C. Nouar, N. Kabouya, J. Dusek, and M. Mamou. Modal and non-modal linear stability of the plane Bingham-Poiseuille flow. *J. Fluid Mech.*, 577:211–239, 2007.

[18] R. Liu and Q.S. Liu. Non-modal stability in Hagen-Poiseuille flow of a Bingham fluid. *Phys. Fluids*, 26:014102, 2014.

[19] N.J. Balmforth, I. A. Frigaard, and G. Ovarlez. Yielding to stress: Recent developments in viscoplsatic fluid mechanics. *Ann. Rev. Fluid. Mech.*, 46:121–146, 2014.

[20] J. E. Mott and D. D. Joseph. Stability of parallel flow between concentric cylinders. *Phys. Fluids*, 11:2065–2073, 1968.

[21] V. Sadeghi and B. G. Higgins. Stability of sliding Couette-Poiseuille flow in an annulus subject to axisymmetric and asymmetric disturbances. *Phys. Fluids*, 3(9):2092–2104, 1991.

[22] L. Preziosi and F. Rosso. Stability of a viscous liquid between sliding pipes. *Phys. Fluids*, 2(7):1158–1162, 1990.

[23] Ph. Gitler. Stability of axial Poiseuille-Couette flow between concentric cylinders. *Acta Mechanics*, 101:1–13, 1993.

[24] S. J. Cowley and F. T. Smith. On the stability of Poiseuille-Couette flow: a bifurcation from infinity. *J. Fluid Mech.*, 156:83–100, 1985.

[25] L.N. Trefethen, A.E. Trefethen, S. C. Reddy, and T. A. Driscoll. Hydrodynamic stability without eigenvalues. *Science*, 261:578–583, 1993.

[26] S.C. Reddy, P.J. Schmid, and D.S. Henningson. Pseudospectra of the Orr-Sommerfeld operator. *SIAM J. APPL. MATH.*, 53:15–47, 1993.

[27] P. J. Schmid and D. S. Henningson. Optimal energy density growth in Hagen-Poiseuille flow. *J. Fluid Mech.*, 277:197–225, 1994.

[28] P.J. Schmid. Nonmodal stability theory. *Annu. Rev. Fluid Mech.*, 39:129–162, 2007.

[29] G. Gallino, L. Zhu, and F. Gallaire. The stability of a rising droplet: an inertialess non-modal growth mechanism. *J. Fluid Mech.*, 786:R2, 2015.

[30] C. Metivier, C. Nouar, and J. P. Brancher. Linear stability involving the Bingham model when the yield stress approaches zero. *Phys. Fluids*, 17:104106, 2005.

[31] A. Meseguer and L. N. Trefethen. A spectral Petrov-Galerkin formulation for pipe flow I: Linear stability and transient growth. *Report, 0xford University*, 18, 2000.

[32] H. Vitoshkin, E. Heifetz, A. Yu. Gelfgat, and N. Harnik. On the role of vortex stretchning in energy optimal growth of three-dimensional perturbations on plane parallel shear flows. *J. Fluid Mech.*, 707:369–380, 2012.

[33] D. D. Joseph and S. Carmi. Stability of Poiseuille flow in pipes, annuli and channels. *Quart. Appl. Math.*, 26:575–599, 1969.

[34] C. Nouar and I. Frigaard. Nonlinear stability of Poiseuille flow of a Bingham fluid: theoretical results and comparison with phenomenological criteria. *J. Non-Newtonian Fluid Mech.*, 100:127–149, 2001.

[35] I. Frigaard and C. Nouar. On three dimensional linear stability of Poiseuille flow of Bingham fluids. *Phys. Fluids*, 15(10), 2003.

[36] J. Peixinho, C. Nouar, C. Desaubry, and B. Théron. Transitional and turbulent flow of yield stress fluid in a pipe. *J. Non-Newtonian Fluid Mech.*, 128:172–184, 2005.

[37] A. Esmael, C. Nouar, A. Lefevre, and N. Kabouya. Transitional flow of a non-newtonian fluid in a pipe: Experimental evidence of weak turbulence induced by shear-thinning behavior. *Phys. Fluids*, 22:101701, 2010.

[38] B. Guzel, T. Burghelea, I. Frigaard, and D.M. Martinez. Observation of laminar-turbulent transition of a yield stress fluid in Hagen-Poiseuille flow. *J. Fluid Mech.*, 627:97–128, 2009.

[39] A. Bottaro, P. Corbett, and P. Luchini. The effect of base flow variation on flow stability. *J. Fluid Mech.*, 476:293–302, 2003.

[40] L. M. Mack. The initial stage of transition in cylindrical pipe flow: role of optimal base-flow distorsion. *J. Fluid Mech.*, 517:131–165, 2004.

[41] G. BenDov and J. Cohen. Critical Reynolds number for a natural transition to turbulence in pipe flows. *Phys. Rev. Lett.*, 98:064503, 2007.

[42] G. BenDov and J. Cohen. Instability of optimal non-axisymmetric base flow deviations in pipe poiseuille flow. *J. Fluid Mech.*, 588:189–215, 2007.

[43] C. Nouar and A. Bottaro. Stability of the flow of a Bingham fluid in a channel: eigenvalue sensitivity, minimal defects and scaling laws of transition. *J. Fluid Mech.*, 642:349–372, 2010.

[44] J.O. Pralits, A. Bottaro, and S. Cherubini. Weakly nonlinear optimal perturbations. *J. Fluid Mech.*, 785:135–151, 2015.